University of Texas at El Paso
ScholarWorks@UTEP

Open Access Theses & Dissertations

2023-05-01

Differentiating Biotic Vs. Abiotic Co2 In The Formation Of Pedogenic Carbonate In Agriculture And Natural Dryland Soils

Valeria Isabel Molina
University of Texas at El Paso

Follow this and additional works at: https://scholarworks.utep.edu/open_etd

 Part of the Geochemistry Commons, Hydrology Commons, and the Soil Science Commons

Recommended Citation

Molina, Valeria Isabel, "Differentiating Biotic Vs. Abiotic Co2 In The Formation Of Pedogenic Carbonate In Agriculture And Natural Dryland Soils" (2023). *Open Access Theses & Dissertations*. 3826.
https://scholarworks.utep.edu/open_etd/3826

This is brought to you for free and open access by ScholarWorks@UTEP. It has been accepted for inclusion in Open Access Theses & Dissertations by an authorized administrator of ScholarWorks@UTEP. For more information, please contact lweber@utep.edu.

DIFFERENTIATING BIOTIC VS. ABIOTIC CO_2 IN THE FORMATION OF PEDOGENIC CARBONATE IN AGRICULTURE AND NATURAL DRYLAND SOILS

VALERIA ISABEL MOLINA

Master's Program in Geological Sciences

APPROVED:

Lixin Jin, Ph.D., Chair

Lin Ma, Ph.D.

Mark Engle, Ph.D.

Anthony Darrouzet-Nardi, Ph.D.

Stephen L. Crites, Jr., Ph.D.
Dean of the Graduate School

Copyright ©

by

Valeria Isabel Molina

2023

DEDICATION

I dedicate this work to my beloved family and loved ones, whose support and encouragement have been a constant source of motivation throughout my academic journey. I also dedicate this to a brighter tomorrow, as I aspire to contribute towards the well-being of our Mother Earth, who provides us with a home to thrive and prosper. May this work serve as a small step towards creating a better future for our planet and all of its inhabitants.

DIFFERENTIATING BIOTIC VS. ABIOTIC CO_2 IN THE FORMATION OF PEDOGENIC CARBONATE IN AGRICULTURE AND NATURAL DRYLAND SOILS

by

VALERIA ISABEL MOLINA, A.S., B.S.

THESIS

Presented to the Faculty of the Graduate School of

The University of Texas at El Paso

in Partial Fulfillment

of the Requirements

for the Degree of

MASTER OF SCIENCE

Department of Earth, Environmental, and Resource Sciences

THE UNIVERSITY OF TEXAS AT EL PASO

May 2023

ACKNOWLEDGMENTS

I would like to express my heartfelt appreciation to my admirable advisor, Dr. Lixin Jin, and my esteemed committee members and colleagues for their invaluable guidance, support, and contributions, which have been instrumental in shaping my research and education.

I am also grateful for the financial support from the NSF Awards #1853680 and #2012475, which provided the foundation for my project, and the Dryland Critical Zone team, JEM group, and GG project, for their innovative research that addresses pressing societal concerns and creates an inclusive environment for passionate students like myself.

I would like to extend my gratitude to my loving friends, family, and Markhos, who have persistently stood by my side and rooted for me despite my limited availability during graduate school, your unconditional support has meant the world to me.

Special thanks go to Michelle Quiroz my dedicated field helper for their invaluable assistance in auguring the sticky clay and the installation of sensors and soil gas samplers at the pecan orchard collecting data, and traveling together to the regional 2021 GSA conference. Thank you, Art and the Jornada Basin LTER for allowing us to contribute to dryland critical zone research.

Once again, I am deeply grateful to all those who have contributed to my academic journey and research endeavors. Your support and encouragement are truly appreciated and will be cherished forever.

ABSTRACT

Drylands, characterized by low and sporadic precipitation, require irrigation for crop growth. However, irrigation practices can lead to salt accumulation in soil due to high evaporation rates and reduced leaching. In addition to loading salts to soil, irrigation promotes the accumulation of secondary calcite. In natural systems, the formation of pedogenic carbonate (secondary calcite, $CaCO_3$) is critical, impacting the soil properties hydrologically and biogeochemically, and modifying the global carbon cycle over geological time, albeit at a lower rate. In agricultural sites, irrigation water supplies HCO_3^- and Ca^{2+}, accelerating the rates of $CaCO_3$ formation and releasing abiotic CO_2. This study investigated the abiotic and biotic processes that have produced soil CO_2 in dryland soils at an irrigated pecan orchard in Tornillo, Texas, and a natural site within Jornada Experimental Range, New Mexico. Two sites within the pecan orchard, Pecan_Coarse, and Pecan_Fine, have contrasting soil textures resulting in different soil salinity, pedogenic carbonate accumulation rates, and tree sizes. A range of methods was employed including CO_2, O_2, moisture sensors, and soil gas samples for pCO_2 and $\delta^{13}C_{CO2}$ measurements, as well as irrigation water collection and analyses at the orchard, for pH, alkalinity, and $\delta^{13}C_{DIC}$. The overall objective of this study is to quantify the release of abiotic CO_2 during the precipitation of irrigation-induced calcite, as a function of spatial variability due to soil texture, and as a function of growing season and irrigation events at a high temporal scale.

Three CO_2 end-members in the agricultural system (the atmospheric, biotic, and abiotic/calcite derived) have their distinctive C isotope signatures. Soil gas samples at Pecan_Fine (> 30 cm), without the influence of atmospheric CO_2, are plotted closer to abiotic CO_2 endmember than those at Pecan_Coarse, due to finer soil texture, more salt buildup, faster calcite accumulation, and thus more abiotic CO_2. In contrast at the Pecan_Coarse, more soil CO_2

is generated biotically, with larger tree sizes, and thus more soil respiration than Pecan_Fine. Two-component mixing model results show that the abiotic process has contributed up to 72% of total soil CO_2 at Pecan_Fine and only up to 47% at Pecan_Coarse. These contributions are much higher than those reported by Ortiz et al. (2022) because local groundwater of much higher total dissolved solids was utilized for irrigation in this study producing more calcite-derived abiotic CO_2 than river water in the previous study. When irrigation sources are switched from local groundwater to river water in the summer, the $\delta^{13}C_{DIC}$ of irrigation water shifts, leading to a corresponding shift in the $\delta^{13}C$ signature of abiotic CO_2.

The temporal variability of soil pCO_2 and pO_2 is driven by irrigation at both Pecan_Fine and Pecan_Coarse soils. After irrigation, water filtration pushes the O_2 out, and when soil pores open up with evaporation, O_2 diffuses in from the atmosphere until the next irrigation. Soil CO_2 behaves differently: irrigation water, at equilibrium with atmospheric CO_2, dissolves soil CO_2 and lowers its concentrations after irrigation. With continuous evaporation, soil water concentrations increase leading to the precipitation of calcite and the release of abiotic CO_2, leading to higher pCO_2. Similarly, supported by higher pO_2, soil respiration rate also is elevated, releasing biotic CO_2 and leading to higher pCO_2. Higher pCO_2 also leads to diffusion loss of CO_2 from soil to the atmosphere. When soil CO_2 production is lower than the overall CO_2 loss, the soil pCO_2 reaches a maximum and begins to drop. Although the temporal trends are similar between two sites of different soil textures, the magnitude of variations in pCO_2 and pO_2 within each irrigation is different, dictated by texture-controlled water and gas transport.

The Jornada Experimental Range provides an opportunity to study the natural dryland ecosystem, wherein rainfall patterns and seasonal variability are the primary factors controlling soil pCO_2 and pO_2. Through this project, we have deepened our understanding of the soil C

budget in both natural and managed drylands by investigating the biotic and abiotic processes that contribute to soil CO_2. Our research has demonstrated that soil CO_2 production in drylands is strongly influenced by soil texture, water inputs, and its corresponding chemical composition. Specifically, the combination of fine soil texture and continuous evaporation can lead to chemical saturation of evaporate minerals, resulting in salt buildup and the formation of pedogenic carbonates, which in turn produce abiotic CO_2. It is critical to comprehend these processes in agricultural soil systems in drylands, as the accumulation of pedogenic carbonates can impact soil health, crop yields, and the global C budget.

TABLE OF CONTENTS

LIST OF TABLES

LIST OF FIGURES

1. INTRODUCTION

Soil inorganic carbon (SIC) is continuously relevant to the long-term geological C cycle and the fast biotic C cycle (Serrano-Ortiz et al., 2010; Zamanian et al., 2016). SIC is as critical as soil organic carbon (SOC), particularly in arid to semiarid climates, since SIC contains the largest C pool (Naorem et al., 2022; Wang et al., 2015; Zamanian et al., 2016). In general, areas with limited water availability and high evapotranspiration rates exhibit higher amounts of soil inorganic carbon (SIC), as these conditions restrict dissolution reactions and the leaching of carbonates from the soil (Zamanian et al., 2016). The highest stocks of SIC are in arid lands where the MAP is less than 250 mm, such as Australia, the Middle East, the Saharan desert (Africa), and the western United States of America (Plaza et al., 2018). In desert soils, SIC is in the form of secondary carbonates via Rxn (1) (Ezcurra & United Nations Environment Programme, 2006; Plaza et al., 2018). The accumulation is slow and thus pedogenic carbonate in soils is visible over thousands of years in the soil Bk layer (Gallagher & Breecker, 2020; Laity, 2008; Zamanian et al., 2016). Pedogenic carbonate exists in many forms, powdery, nodular, or highly indurated (Durand et al., 2018; Zamanian et al., 2016). It is estimated that calcretes are widely distributed, covering ~13% of the earth's terrestrial surface (Laity, 2008).

$$Ca^{2+} + 2HCO_3^- \leftrightarrow CaCO_{3(s)} + CO_{2(g)} + H_2O \qquad \text{Rxn (1)}$$

Zamanian et al. (2016) observed that climate is the major condition affecting the depth and likelihood of pedogenic carbonate formation especially the seasonal distributions of precipitation with a minor contribution of temperature that modifies the rates of evaporation and governs the dominant biome (e.g. hot deserts and cold tundra). Laity (2008) suggested that calcium carbonate precipitated at warmer temperatures, because lower CO_2 solubility at higher temperatures drives the supersaturation of soil water with calcite (Zamanian et al., 2016). Although rising temperatures

also increase microbial respiration rates, the latter increases pCO_2 in soil gas contributing to the "abiotic effect of CO_2 solubility" (Gocke et al., 2011; Zamanian et al., 2016).

Drylands which cover ~40% of the Earth's land, sustain ~40% of the human population (Liu et al., 2015; Plaza-Bonilla et al., 2015; Reynolds et al., 2007). As the population continues to grow, the demand for food and usable water has escalated (Cox et al., 2018; Hannam et al., 2019). Unfortunately, the buildup of salts in irrigated dryland soils is a global predicament and leads to soil degradation (Cox et al., 2018; Laity, 2008; Ortiz et al., 2022; Ortiz & Jin, 2021). High evapotranspiration rates and irrigation water with high total dissolved solids (TDS) promote precipitation of salts, even most soluble evaporites (e.g., halite and gypsum) along with less soluble calcite (pedogenic carbonate) (Rxn (1); Nyachoti et al., 2019). Agriculture, i.e., the application of irrigation water is expected to affect the accumulation rates of pedogenic carbonate and the sequestration of C (Nyachoti et al., 2019). This issue is related to the availability of calcium and bicarbonate ions provided by irrigation water which could therefore exceed calcite saturation (Nyachoti et al., 2019). The accumulation of pedogenic carbonate in soil could further affect the soil properties by reducing porosity, infiltration, root growth, fluid mobility, and more importantly the release of abiotic CO_2 (Ortiz et al., 2022).

Soil respiration is considered to be a significant component of the global C cycle (Angert et al., 2015), and includes organic matter degradation, root respiration, and microbial respiration (Rxn (2); Rey, 2015; Gallagher & Breecker, 2020). The respiration process consumes O_2 to produce CO_2 (Gallagher & Breecker, 2020; Hodges et al., 2019):

$$CH_2O_{(om)} + O_2 \leftrightarrow CO_{2(g)} + H_2O \qquad \text{Rxn (2)}$$

2. MY DRIVING QUESTIONS: DIFFERENTIATING SOURCES OF CO_2 IN NATURAL AND IRRIGATED DRYLAND SOILS.

This project will differentiate biotic and abiotic CO_2 in drylands and uncover the processes contributing to CO_2 and pedogenic carbonate formation in agricultural and natural soils by analyzing O_2/CO_2 gas concentrations, volumetric water content, C isotopes, and irrigation water chemistry. I hypothesize that after each irrigation, soil water will be concentrated by evaporation, especially in finer-textured soils, releasing abiotic CO_2, detectable by both C isotopes and also coupling of CO_2/O_2 sensors. Explicitly, I want to investigate agricultural sites in drylands that are more biologically active yet might have more abiotic processes releasing soil-respired CO_2 than previous studies have assumed. Guided by the conceptual diagram in Figure 1, my driving questions were:

- Does the relative contribution of soil CO_2 from biotic or abiotic processes change spatially (soil texture) and temporally (irrigation event)? How is this different from the soil in natural versus irrigated dryland?
- Is the source of soil CO_2 in dryland related to the water inputs (rainfall, and river versus groundwater irrigation) and their varying elemental chemistries?

3. STUDY AREAS

3.1 Natural Dryland Study Area

Our natural study area is located on a piedmont slope within the USDA Jornada Experimental Range in southern New Mexico, further referred to as JER_VM (Figures 2A and 2B). This study area has been scientifically investigated, as part of the dryland Critical Zone project. The natural terrain has diverse land morphologies with varying surface stabilities, and different land features such as areas of desert pavements, arroyos, soil crust, and vegetation cover (Figures 2A and 2B). Dryland soils contain abundant secondary pedogenic carbonate that exists in various stages of development (Durand et al., 2018; Nyachoti et al., 2019); at JER_VM it ranges from filaments and nodular structures to thick laminae deposits (Nyachoti et al., 2019).

A soil map from the Web Soil Survey (WSS) of the United States Department of Agriculture (https://websoilsurvey.nrcs.usda.gov/app/) was used to identify the major soil units present in the Experimental Range, NM study area (Appendix Figure 1A). The dominant soil unit at the piedmont slope (labeled as unit 26) is Doña Ana and Chutum complex and has slopes ranging from 1 to 10%. JER_VM site, where the sensors and gas samplers were installed for this study, belongs to this unit (Figure 2B). The remaining 26% of the study area, labeled as unit 56, includes the Mimbres, Chutum, and Ybar complex with slopes ranging from 0 to 5%. Our study investigates soil processes at 15 and 30 cm at JER_VM, which would lie within the B_W soil horizon (weathered B-horizon) and has been classified as a sandy loam to clay loam texture.

3.2 Agricultural Dryland Study Area

Along the arid southwestern U.S., there is an extensive network of ditches and canals diverting river water from the Rio Grande, the main source for irrigating fields (Cox et al., 2018). The primary issue is the use of water with high salinity for irrigation, impacting the finer soil conditions that are directly observable by reduced crop yields (Doser et al., 2019; Ganjegunte & Braun, 2011). The soils with finer texture have a slow infiltration rate potentially leading to ponding of water; the excess water is subsequently evaporated, precipitates salts, and impacts crop yields (Cox et al., 2018). In early spring, fields are flushed in an attempt of dissolving salts and moving them to groundwater (Ortiz and Jin, 2021).

This study area is a pecan field in Tornillo, Texas owned by the Ivey family (Figure 2C). The orchard, referred to as the pecan orchard is seasonally flood-irrigated approximately once about every 2-3 weeks (Ganjegunte & Braun, 2011) from April to October. The parent material of the sediments which fill the basin is the Rio Grande River Holocene fluvial deposits (Doser et al., 2019), characterized by heterogeneous soil texture horizontally and vertically. Two sites have been selected on extreme endmembers of soil texture and tree size: Pecan_Fine with mostly silt and clay particles, more salt buildup and smaller trees, and Pecan_Coarse with a more sandy texture, lower salt buildup, and bigger trees (Figure 2C; Appendix Figure 1B). The growth of trees is significantly impacted by soil salinity and soil texture, as they control the potential water supply available to the tree roots and also the tree root distribution (Miyamoto et al., 1986). Although the field is predominantly irrigated by the local river water, surface water volumes can be scarce and the farmers improvise by substituting it for more saline local groundwater from the alluvial aquifer system underlying the farms.

Similarly, to JER_VM, a soil map was produced with the USDA's WSS for our agricultural study area. In comparison, the pecan orchard has high textural variability as there are a total of 6 map unit groups (Appendix Figure 1B), ranging from silty clay loam (73.3%), silty clay (25.5%), loam (0.8%), and fine sandy loam (0.4%). The top 3 map units at the pecan orchard include the Saneli silty clay loam (52%), Tigua silty clay (25.5%), and Harkey silty clay loam (15%). However, the Pecan_Coarse site is located at the Glendale silty clay loam (Ge) which is only 6.3% of the total pecan orchard while the Pecan_Fine site is within the Tigua silty clay (Tg; Figure 2B). The Tg soil unit landform is floodplains with parent material composed of Holocene clayey alluvium. The top 25.4 cm of the soil profile is classified as silty clay, then below from 25.4 to 127 cm is clay, and silt loam from 127 to 152.4 cm. The Tg unit has moderately well drainage with high runoff and a calcium carbonate, maximum content of 5%. The Ge unit landform is also floodplain but with Holocene fine-silty alluvium parent material. The top 89 cm of the soil is silty clay loam, from 89 to 152.4 cm the soil has been classified as stratified fine sand to silty clay loam. Here the drainage is well with low runoff and a maximum calcium carbonate content of 10%.

4. METHODOLOGY

An array of sensors, in addition to soil gas and soil water samplers, were utilized at three different sites (JER_VM, Pecan_Coarse, and Pecan_Fine) (Table 1; Figure 3) to differentiate and investigate the biotic and abiotic soil CO_2 production in both managed and natural dryland areas.

4.1 Sensors

Three variables are monitored by sensors, volumetric water content (VWC), partial pressure of O_2 (pO_2), and partial pressure of CO_2 (pCO_2) in the soils of three sites (Table 1). The O_2 sensors (Apogee) and CO_2 sensors (eosGP, eosense) are coupled and installed at 30 and 60 cm at Pecan_Fine and Pecan_Coarse sites, and at 15 cm and 30 cm at the JER_VM site, which are above the caliche layer (~40 to 60 cm deep). For soil moisture (VWC), ECH_2O 5TE (METER) sensors were installed at 30 and 60 cm while the TEROS 12 (METER) sensors were later installed at 90, 120, and 150 cm in Pecan_Fine and Pecan_Coarse sites; CS650 (Campbell Scientific) were employed at JER_VM at 15 and 30 cm, as these TDR-based sensors work better in dry conditions, have a larger measurement volume and less impacted by preferential flow in rocky terrain.

4.1.2 Sensor Calibrations

At our pecan orchard sites, ECH_2O 5TE soil moisture sensors with SDI-12 communication were used to obtain raw dielectric output, EC, and raw temperature values (Hilhorst, 2000). Raw values were then converted to standard units using a Matlab code. This conversion process involved converting raw dielectric output to dielectric permittivity, and temperatures to Celsius, and then applying the Topp equation to derive the volumetric water content values. The 5TE sensor utilizes an electromagnetic field to measure dielectric permittivity by applying a 70 MHz

oscillating wave to the sensor prongs that are charged by the dielectric of the soil material (Topp et al., 1980). The charge corresponds to the dielectric and VWC of the soil medium, which is how the sensor micro-processes and measures the charge and provides the output of the dielectric permittivity. Before installation at the orchard sites at depths of 30 and 60 cm, the sensors were tested underwater in a lab to ensure accurate readings.

TEROS 12 soil moisture sensors were installed at depths of 90, 120, and 150 cm at the same pecan orchard sites. These sensors were connected to a METER ZL6 data logger, which provided instantaneous data upload to ZENTRA Cloud. The TEROS 12 sensors are insensitive to soil texture and EC variations, and their generic calibration equation ensures accurate measurements. VWC values were obtained from the dielectric permittivity measurements using the Topp equation in the ZENTRA Cloud.

The soil moisture sensors used at the JER_VM site are the Campbell Scientific CS650 models, which are designed as water content reflectometers with two parallel 30 cm stainless steel rods. These sensors were chosen for their TDR-based technology, which is less impacted by heterogeneous paths and works well in dry soil conditions. The sensors operate by measuring the velocity of electromagnetic wave propagation, which is influenced by the dielectric permittivity of the surrounding material (Topp et al., 1980). In order to derive volumetric water content (VWC) values, a Matlab code is used to calculate the dielectric permittivity from the signal attenuation and oscillation period and then applies the Topp equation.

The Apogee SO-110 oxygen soil gas sensor was calibrated and tested in the lab before installation. A two-point calibration was performed by measuring the millivolts value of the sensor outdoors in air and then submerging it in water to simulate anoxic conditions. The sensor is of the galvanic cell type and includes a Teflon membrane, reference temperature sensor, internal

resistance heater, and signal processing circuitry. Since the oxygen concentration decreases with decreasing barometric pressure due to elevation, absolute oxygen measurements can provide information on biological and chemical processes. As barometric pressure decreases with elevation, the oxygen concentration also decreases. To convert the sensor raw data to relative oxygen concentration, a linear calibration factor is calculated and used.

The eosGP CO_2 sensor features a gas-measuring membrane that exhibits high resistance to abrasion and low water absorption, with an accuracy of approximately 1% of measured values. These sensors were calibrated by the manufacturer using a two-point calibration curve, with calibration parameters dependent on whether the sensor had single or dual-range capabilities measuring high CO_2 (0-12.5%) or low CO_2 (0-5%). Sensors with higher capacity ranges were used for deeper soil depths, while sensors with lower concentration ranges were installed at shallower depths since greater soil depths typically are characterized by higher CO_2 concentrations. Atmospheric conditions were maintained during readings, and the millivolt values obtained were converted to ppm using the calibration equation provided by the manufacturer.

4.2 Gas Sample Collection and Analyses

Soil gas samplers were prepared according to a modified USGS protocol (Hasenmueller et al., 2015; Jin et al., 2014). Three nets of samplers were installed at 30, 60, and 100 cm at Pecan_Fine and Pecan_Coarse sites, and at 15 and 30 cm at JER_VM (Table 1). Each gas sample was collected from the sampler after purging, using a syringe and needle, extra stopcock, and injected into pre-evacuated 15 mL glass vials (LETCO). A total of 6 samples were collected at JER_VM and 133 samples were collected at the pecan orchard in 2021. Samples were analyzed for pCO_2 and $\delta^{13}C_{CO2}$ at the Stable Isotope Facility at the University of California at Davis. CO_2

was pushed out of the sample vial using helium carrier gas, and analyzed by a Thermo Scientific GasBench II coupled to a Thermo Finnigan Delta Plus XL isotope-ratio mass spectrometer (IRMS) (Tu et al., 2001). Reference gases were run for quality control and quality assurance every 10 samples, and the measurement error is ± 0.10‰ for $\delta^{13}C_{CO2}$ and ± 0.20‰ for $\delta^{18}O_{CO2}$. Peak areas were used to calculate CO_2 concentrations using four standards of various concentrations: 400, 3000, 10000, and 50000 ppm (v). The relative standard deviation for replicates of each gas standard is usually better than 0.1%.

4.3 Sampling of Irrigation Water at the Pecan Orchard:

A total of 8 irrigations by groundwater and river water were applied to the pecan orchard in the year 2021. Four irrigation water samples were collected from the main canal that is adjacent to the pecan orchard in 2021: 3 by the river and 1 by groundwater (Appendix Table 1). The pH and electrical conductivity (EC) values of these water samples were measured on-site. Specifically, the Thermo Scientific Orion 3 Star Meter was utilized to measure the EC, after two points of calibration (1413 µs/cm and 12.9 ms/cm). Two distinct meters were calibrated by a pH 7 buffer and then a pH 4 buffer: sympHony model SP70P and the Thermo Electron - Orion STAR A325. Water samples were measured for alkalinity, $\delta^{13}C_{DIC}$, and water isotopes. Gran alkalinity was titrated by dilute HCl using the Mettler Toledo DL15, and the absolute molarity of this HCl was titrated using standard solutions made from pure $NaHCO_3$.

The $\delta^{13}C_{DIC}$ were analyzed at the Stable Isotope Facility at the University of California at Davis, with a precision of ± 0.10 ‰. The water isotopes ($^2H/^1H$ and $^{18}O/^{16}O$) of each irrigation water sample were measured six times using a vaporizer and autosampler on the Picarro L2130-I ring-down spectroscopy (Gardea, 2022). The isotope ratios of samples are normalized to the

Vienna Standard Mean Oceanic Water (VSMOW). The instrument was calibrated by three standard solutions, namely, zero (consisting of seawater with $\delta^{18}O$=0.3‰ and $\delta^{2}H$=1.8‰), mid ($\delta^{18}O$= -20‰ and $\delta^{2}H$= -150‰), and depleted ($\delta^{18}O$ = -29‰ and $\delta^{2}H$= -235‰).

4.4 Rainfall Data

The precipitation data were obtained from the National Oceanic and Atmospheric Administration's Climate Data Online (CDO). For the pecan orchard the daily summary records between May 26 and November 2, 2021, were selected to correspond with the duration of the sensor measurements during the irrigation season. The data were derived from the TORNILLO 2 SEE, TX US station (with code USC00419088). For the JER_VM, the precipitation data were from the Jornada Experimental Range, NM US station (with code USC00294426), to match the period of sensors from August 27, 2021, to April 1, 2022 (Appendix Table 2).

5. RESULTS

5.1 Soil Moisture Dynamics

A total of 6 flood-irrigation events were recorded in the growing season of 2021 after the sensor installation, the first and last by groundwater and the remaining 4 by the Rio Grande River (Appendix Table 1). The soil moisture responded immediately in all depths (30, 60, 90, 120, and 150 cm) to irrigation, and natural precipitation, especially during the monsoon season (from July to October) (Figures 4A and B). After irrigation, soil moisture content decreased steadily as the soil became drier and thus lost moisture (Figures 4A and B).

Flood irrigation events at the Pecan_Fine site saturated the soil (e.g., September 2021, irrigation #7 as seen in Appendix Table 1), causing the VWC to plateau at ~ 0.5 cm^3/cm^3 for up to 5 days (Figure 4B). On the other hand, at the Pecan_Coarse site, the VWC never reached a plateau for all observed depths at the same time. However, at 150 cm deep the VWC reached a maximum value of ≈ 0.45 cm^3/cm^3 also after irrigation #7, although this was not a frequent pattern due to the rapid decrease in VWC in Pecan_Coarse. The maximums at Pecan _Coarse after irrigations averaged ~ 0.35 cm^3/cm^3 (Figure 4A). Compared to the Pecan_Fine site, soil moisture values at the Pecan_Coarse site decreased more quickly after irrigations, indicating faster infiltration rates.

At the JER_VM site, VWC responded after each rainfall event, especially the major ones (> 0.1 inches; Figure 4C). The VWC at 15 cm in the soil is predominantly lower than at 30 cm, and also exhibited more variability, showing values between ≈ 0.025 cm^3/cm^3 and up to ≈ 0.05 cm^3/cm^3, while at 30 cm there is a smaller range from ≤ 0.04 cm^3/cm^3 to ≥ 0.05 cm^3/cm^3 (Figure 4C).

5.2 Temporal Variation of Soil pO_2

After an irrigation event or receiving precipitation, soil pO_2 at the pecan orchard sites decreased and went as low as 1% at Pecan_Coarse and reached 0% at Pecan_Fine (Figures 5A and B). A few days following irrigation (≤ 5 days), pO_2 increased until the next irrigation or rainfall event. After the irrigation season ended in late September (irrigation #8), soil pO_2 returned to resemble the atmospheric value (~ 21%), ≈ 10 days or later. In comparison to Pecan_Coarse, soil pO_2 at the Pecan_Fine site typically experienced a sharper decline after flood irrigation (Figure 5B). At both sites, soil pO_2 at 30 cm recovered more quickly than those at the 60 cm depth. At Pecan_Coarse, pO_2 at 30 and 60 cm were more similar in comparison to those at Pecan_Fine (Figures 5A and 5B).

In the case of both Pecan_Coarse and Pecan_Fine, following each irrigation, the concentration of O_2 is depleted to a greater extent at 30 cm than at 60 cm depth (Figures 5A and 5B). However, the rate of recovery of O_2 concentration at 30 cm depth is faster due to its shallower depth and its proximity to the atmosphere, enabling rapid O_2 exchange with the atmosphere through diffusion. The abrupt decline in O_2 concentration after each cycle suggests that water flooding the field physically displaces O_2 soil gas, causing it to evacuate out of the soil profile but to different degrees depending on the soil texture.

Soil pO_2 at the JER_VM site showed less variability with time than those in the pecan orchard (Figure 5C). For the seven months where data were available, soil pO_2 was slightly lower in the early spring than in the winter. A larger variability was observed at 15 cm depth (≈ 18% to ≥ 21.5%), than at 30 cm depth (> 18% to > 21.5%). Precipitation has only a minor effect on the soil pO_2 (Figure 5C).

5.3 Temporal Variation of Soil pCO_2

Soil pCO_2 at the pecan orchard varied temporally as a function of flood irrigation (Figures 6A and B). Within each irrigation cycle at both Pecan_Fine and Pecan_Coarse sites, the soil pCO_2 showed similar general trends: it decreased with irrigation, gradually increased, and then reached maximum CO_2 concentration; after that, CO_2 decreased slowly until the next irrigation, although the concentrations were different overall. Pecan_Coarse had lower CO_2 concentrations at 30 cm, reaching ≈ 1% and the highest concentrations reached ≥ 7% at 60 cm. In contrast, at Pecan_Fine, the minimum concentrations among both depths 30 and 60 cm were similar, however in general at 60 cm the CO_2 concentrations were lowest (≤ 1%) but also experienced the highest (6%).

During the monsoon season with intensive rainfalls, there were multiple peaks within an irrigation cycle thus multiple rising and falling limbs. Soil pCO_2 also behaved differently between the two sites at the pecan orchard, after rain events in mid-August Pecan_Fine reached low concentrations of ≈ .5%, while in Pecan_Coarse concentrations were kept at ≥ 3%. At Pecan_Fine, the peak soil pCO_2 was reached typically ≈ 10 days after the field was flooded (Figure 6B); while for Pecan_Coarse it occurred sooner, often within the same week of flood irrigation (Figure 6A). Between the two sites, larger differences in pCO_2 were observed between 30 and 60 cm depths at Pecan_Fine than at Pecan_Coarse (Figures 6A and B).

Soil CO_2 at the JER_VM site was not as dynamic as our irrigated system (pecan orchard). From August to October of 2021 (late summer/early fall), the highest soil pCO_2 peak was observed in late August reaching 2% at 15 and 30 cm depth (Figure 6C). Then a second peak occurred in late September when rain events were most abundant and frequent. Smaller peaks were also visible in the colder months subsequently coinciding with precipitation events each time. Generally, pCO_2 was higher at 15 cm than at 30 cm at the JER_VM site (Figure 6C).

5.4 pCO_2 and $\delta^{13}C_{CO2}$ of Soil Gas Samples

Soil pCO_2 measured from physical gas samples was plotted in conjunction with sensor data, and they agreed well (Figures 6A and 6B). The soil pCO_2 increased with depths (Figure 7A), much higher than atmospheric pCO_2 (≈ 0.04%). At Pecan_Fine 100 cm pCO_2 reached ≈ 5% to ≈ 8.5%, but only ≈ 3.5% to ≈ 6.5% at Pecan_Coarse (Figures 6A and 6B). Figure 7A indicates that Pecan_Fine is in general higher in CO_2 concentrations, especially true at 8 am versus 10 pm. The $\delta^{18}O_{CO2}$ showed no clear depth trend and ranged from 32‰ to 36‰ (Figure 7B). The $\delta^{13}C_{CO2}$ did not change much with depth but varied slightly: $\delta^{13}C_{CO2}$ signatures were more depleted at Pecan_Coarse than at the Pecan_Fine site (Figure 7C). Atmospheric $\delta^{13}C_{CO2}$ was much less negative than those of soil gases.

5.5. Irrigation Water Chemistry

Irrigation waters (river and groundwater) were relatively alkaline, with pH ranging from 7.4 to 7.8 and alkalinity ranging from 3.7 to 4.7 meq/kg (Appendix Table 1). The EC values varied from 1.09 to 1.97 mS/cm for the river samples, much lower than that of the groundwater sample (3.88 mS/cm) (Appendix Table 1). The $\delta^{13}C_{DIC}$ of two groundwater samples (collected on the same date but at two separate locations along the canal), was at -12.1‰ and -12.4‰. The $\delta^{18}O$ signatures for the river water samples ranged from -6.68‰ to -6.76‰, while the groundwater sample showed a lower value of -8.63‰.

6. DISCUSSION

6.1 Soil Textures Control Hydrological, Biological, and Geochemical Processes

The dryland ecosystem has low biological activity due to limited rainfall and sparse vegetation coverage (Muscolo et al., 2011; Sidari et al., 2008); indeed soils at JER_VM are characterized by low moisture, low pCO_2, and high pO_2 (Figures 4C, 5C and 6C). Only after sporadic precipitation events, does soil moisture slightly increase (Figure 4C) along with a slight increase in O_2 and correspondingly CO_2 increase (Figures 5C and 6C). Soil moisture at 30 cm depth is greater than that at 15 cm (Figure 4C), probably because soils at 30 cm are right above the pedogenic carbonate layer (~40 - 60 cm), a porous moisture-retaining barrier, and in contrast, soil moisture levels are lower at 15 cm by evapotranspiration near the surface (Figures 3B and 4C).

In contrast to the natural ecosystems, irrigation, on top of rainfall, makes the pecan orchard more hydrologically active (Figures 4A and 4B). Interestingly, the soil moisture dynamics are different between the two sites of different soil textures. At Pecan_Coarse, soil moisture (VWC) reached a maximum of ≈ 0.45 cm^3/cm^3, lower than that observed at Pecan_Fine, ≈ 0.55 cm^3/cm^3, although estimated bulk density and porosity are similar between the two sites at the surface (BD = 1.2 to 1.3 g/cm^3, and porosity= 49-55%; Figures 4A and 4B). This discrepancy can be attributed to the varying rates of infiltration and evapotranspiration processes with different soil textures. The soil moisture decreases gently at Pecan_Fine after each irrigation cycle, suggesting that infiltration rates are typically sluggish, and evaporation and transpiration rates are low (Figure 4B). In contrast, at Pecan_Coarse after the irrigation events, soil water moves down quickly and drains faster (Figure 4A). The relative proportion of infiltration versus evapotranspiration controls salt loading. Indeed, more salts are accumulated after 100 years of soil cultivation at the Pecan_Fine site than at the Pecan_Coarse site, especially above the finer layer at depths of 100 - 150 cm (Ortiz

and Jin, 2021). Similarly, higher pedogenic carbonate contents are observed at Pecan_Fine than at Pecan_Coarse (Ortiz et al., 2022).

Just like soil moisture contents, the soil pO_2 varies primarily as a function of irrigation or rainfall events. The soil pO_2 decreases quickly with water inputs, especially in the pecan orchard (Figures 4A, 4B, 5A, and 5B): Soil pO_2 levels drop to 1% at Pecan_Coarse and even become zero at Pecan_Fine (Figures 5A and 5B). O_2 behaves also differently at Pecan_Fine and Pecan_Coarse. Irrigation water moves quickly through the coarser particles at the Pecan_Coarse, leaving a fraction of soil pores filled by the gas phase including O_2, but at Pecan_Fine, soils could be saturated by water without a gas phase and pO_2 is 0%. Furthermore, at Pecan_Coarse, pO_2 at 30 and 60 cm depths recover quickly after irrigation and also are similar in concentrations, indicating fast diffusion of O_2 from air to deeper soils within a coarser soil texture. At Pecan_Fine, as the soil dries after irrigation, mud cracks form on the surface due to the swelling and contraction of expansive clay particles (Laity, 2008), enabling and facilitating atmospheric O_2 to enter the shallow depths, here seen at 30 cm within the soil. However, the diffusion of O_2 to deeper depths is limited by the finer soil texture and lower gas permeability, as observed by the longer time for reestablishing pO_2 back to the atmospheric level at 60 cm soil (Figure 5B).

The availability of O_2 is very crucial for soil respiration (Hillel, 1980; Kramer & Boyer, 1995; Rosenberg et al., 1983): crop yield and root growth are shown to suffer if soil gas pO_2 is less than 15%, especially in agricultural fields. Thus, it is reasonable to assume that respiration rates are also much lower when O_2 is lower in soil and that Pecan_Coarse soils respire faster than Pecan_Fine soils due to O_2 limitation.

Rainfall makes the dryland soils more biotically active through respiration as evidenced by slightly higher pCO_2 during the summer monsoon season (Figure 6). This is more obvious in the

agricultural field: irrigation drives both soil respiration (Rxn (2)) and calcite precipitation (Rxn (1)), producing much higher CO_2 in agricultural soils than in natural soils (Figure 6A and B; Ortiz and Jin, 2021; Ortiz et al., 2022). Both sites in the pecan orchard exhibit higher CO_2 concentrations in the soil at a depth of 60 cm (Figures 6A and B). Notably at 60 cm, Pecan_Coarse displays greater fluctuations in CO_2 concentration values and reaches a peak of > 7% in mid-July, whereas Pecan_Fine trends are more stable and reach up to 6% when considering only sensor data. However, when analyzing gas samples from different depths (30, 60, and 100 cm), Pecan_Fine at a depth of 100 cm shows a concentration exceeding 8%, whereas Pecan_Coarse samples at the same depth and time show concentrations exceeding 6%. These results are indicative of the convenience sampling method used to capture soil CO_2 concentrations, and the inconsistency in the timing of peaks during irrigation cycles across both sites suggests that gas sampling may have missed the highest peak observed in Pecan_Coarse during July (Figure 6A and 6B).

At shallower depths, the soil is diffusing CO_2 into the atmosphere to achieve equilibrium between concentration gradients, resulting in lower CO_2 concentrations ($\approx$ 1%). Conversely, higher CO_2 concentrations are expected at greater depths in the soil, as the concentration tends to be much higher than the atmospheric level of ~400 ppm (0.04%) and increases with depth in the soil (see Figure 7A). Therefore, once the field decreases more than 50% in soil moisture physical displacement of soil gas CO_2 caused by water occupying soil pore spaces is no longer the primary contributor instead the CO_2 falling limb is depicting diffusion. Following the last irrigation event, we observe a reduction in CO_2 concentrations to approximately 1% at 30 cm and around 2% at 60 cm (Figures 6A and 6B).

The soil CO_2 concentrations at the JER_VM site exhibit subtle fluctuations, except for notable spikes that occurred following sensor installation in August and again after mid-October.

Following the initial high CO_2 concentration, data indicates levels of approximately 0.5% CO_2, with occasional peaks occurring in response to precipitation events (Appendix Table 2B). The CO_2 concentration peaks appear to be linked to moisture inputs, implying that moisture directly influences CO_2 production. Additionally, biotic processes appear to be more active at depths of 30 and 60 cm, as evidenced by a gradual decrease in the jagged O_2 values (as O_2 is consumed and CO_2 is produced; Figures 5C and 6C). While proper stoichiometry measures have not been employed to investigate this phenomenon, it is a plausible factor contributing to the observed soil gas dynamics over the time series.

6.2. Evaluating the Relative Contribution of Soil CO_2 by Biotic Versus Abiotic processes using C isotopes

To differentiate sources of CO_2, coupled C isotopes and pCO_2 are used through keeling plots (Ortiz et al., 2022). Three end-members are important at the pecan orchard: biotic (soil-respired) CO_2, abiotic (calcite-derived) CO_2, and atmospheric CO_2. Ortiz et al. (2022) characterized these end-members at the same orchard and reported these end-member isotope values. This study, however, is slightly different: irrigation water was entirely from the Rio Grande in 2016 (as reported by Ortiz et al. (2022)), but in 2021, when soil gases were collected for this project, a mixture of the Rio Grande River water and groundwater (GW) was used. As such, Ortiz et al. (2022) were followed to calculate C isotope ratios of abiotic CO_2 from $\delta^{13}C_{DIC}$ of GW. This is described below. The carbon isotopic compositions of the produced $CaCO_3$(s) along with CO_2(g) in Eq. (1) should depend on the carbon isotope composition of irrigation water DIC according to Rayleigh fractionation.

$$\delta^{13}C_{DIC} * DIC = \delta^{13}C^{CO2} * [CO_2] + \delta^{13}C_{CaCO3} * [CaCO_3] \quad (1)$$

While $[CO_2] = [CaCO_3] = 1/2$ DIC (2)

Assuming the temperature is 25°C the ^{13}C fractionation factor (Clark & Fritz, 1997) between $CaCO_3$- CO_2 is 11.1‰: $\delta^{13}C_{CaCO3} - \delta^{13}C_{CO2} = 11.1‰$ (3)

Thus $\delta^{13}C_{DIC}$ * DIC=½ DIC * ($2\delta^{13}C_{CaCO3} - 11.1‰$) (4)

Given that $\delta^{13}C_{DIC} = -12.25‰$ (GW),

The groundwater-derived calcite and CO_2 should have the following isotope ratios:

$\delta^{13}C_{CaCO3} = (-24.5+11.1)/2 = -6.7‰$; $\delta^{13}C_{CO2} = -17.8‰$.

For the river samples, the values produced by Ortiz et al. (2022) were used: $\delta^{13}C_{DIC} = -7.3‰$, $\delta^{13}C_{CaCO3} = -1.75‰$; $\delta^{13}C_{CO2} = -12.85‰$.

This calculation shows that the change of irrigation water source from the Rio Grande River to the local groundwater will shift the isotope ratio of abiotic CO_2 endmember from -12.85‰ to -17.8‰.

The Keeling plot shows that the atmospheric samples (ATM) collected above the soil surface represent the atmospheric CO_2 end-member, indicating a strong influence of other endmembers due to soil CO_2 emission (Figure 8). Soil gases from the Pecan_Coarse have a greater influence on biotic CO_2 production, whereas those at Pecan_Fine are closer to the abiotic CO_2 (GW) endmember (Figure 8). This difference is consistent with the study by Ortiz et al. (2022), where larger pecan trees and higher soil respiration were observed at Pecan_Coarse, while faster pedogenic carbonate accumulation and more abiotic CO_2 were found at Pecan_Fine. This project adds further evidence to support this finding, and in addition to small tree sizes and limited root density, the lower O_2 level at Pecan_Fine also restricts soil respiration.

The contribution of the abiotic process to the overall soil CO_2 production (X_A) can be quantifiable using a two-component endmember mixing equation following Ortiz et al. (2022):

$$X_A = (R_{mix} - R_B) / (R_A - R_B) \quad (5)$$

Where R_A, R_B, and R_{mix} are $\delta^{13}C_{CO2}$ of end-member A (abiotic CO_2), end-member B (Soil respired CO_2), and the mixture (gas samples collected at the pecan orchard). To minimize the influence of atmospheric CO_2, we focused exclusively on deeper depths (60 cm and 100 cm; Figure 8). Irrigation water was from both Rio Grande and groundwater in 2021 for this study, so X_A values were computed separately for gas samples collected after groundwater irrigation and also for river water (groundwater R_A $\delta^{13}C_{CO2}$= −17.8‰; river water R_A $\delta^{13}C_{CO2}$= −12.85‰). Average R_{mix} ($\delta^{13}C_{CO2}$) and its corresponding X_A values, along with their associated standard deviations are reported in Tables 2A and 2B.

To better understand the spatial and temporal heterogeneity of biological versus abiotic processes in contributing to soil CO_2, statistical analyses were conducted through the generation of boxplots and the execution of t-tests, to properly compare X_A values across contrasting different soil textures (Pecan_Fine versus Pecan_Coarse), different depths (30 cm versus 60 cm), and different irrigation water (groundwater and Rio Grande river water; Figure 9). At the pecan orchard, the initial three irrigations for the year 2021 are sourced from the local groundwater and then switch to the Rio Grande River on irrigation #4 on June 15, 2021. The Rio Grande River remained the only water supply until September 20, 2021, the last recorded irrigation cycle reverted to utilizing groundwater.

X_A values are significantly higher at Pecan_Fine soils than at the Pecan_Coarse soils (Figure 9), highlighting the predominant control of soil texture on the CO_2 sources. Within each site, different depths can also behave differently. Specifically, when groundwater is used as the irrigation water source, soil gases at 60 cm and 100 cm are significantly different at the Pecan_Fine site but similar at the Pecan_Coarse (Figure 9A). Indeed, X_A is higher at 100 cm, than 60 cm at

the Pecan_Fine site when irrigated with groundwater, probably indicative of more calcite precipitation at deeper soils, where finer texture is located and a higher abundance of both salt and calcite is observed (Ortiz and Jin, 2021; Ortiz et al., 2022). However, at Pecan_Coarse, this deeper source of abiotic CO_2 is less important, and the higher permeability of coarser grains makes it easy to mix the gases from different depths. Interestingly, after switching to river water, no significant differences are observed in X_A values between 60 and 100 cm depths at Pecan_Coarse or Pecan_Fine (Figure 9B).

However, there are additional factors that may potentially influence the production of CO_2 and its source. Firstly, local groundwater has higher TDS (Ca^{2+} and HCO_3^-) content than river water, producing more pedogenic carbonate and abiotic CO_2. Secondly, the timing of groundwater utilization was early spring, whereas river water became available for irrigation in summer, suggesting a possible influence of seasonality as spring and summer conditions also affect the growth cycles of pecan trees. Thirdly, it is difficult to determine how long signals of one irrigation type (e.g., groundwater) persist when switching to another irrigation type (e.g., river). We do know however that the initial irrigations for the year 2021 were groundwater derived, meaning we can trust the calculated endmember values for the groundwater as it was the first to be introduced to the pecan orchard. The same cannot be said about the river water endmember since there could be mixing in the soil with the previous groundwater since the soil moisture (VWC) is never at 0 cm^3/cm^3 during the irrigation season (Figure 4A and 4B). Because of these factors and data limitations, we only use our statistical analysis as a guide rather than a definitive answer to the abiotic CO_2 contributions.

6.3. Identifying the Primary Controls on CO_2 Production and Transport at the Orchard by Coupling of pCO_2 and pO_2

High-resolution pCO_2 and pO_2 data can allow us to investigate CO_2 production and transport at the pecan orchard. A conceptual framework is presented to depict the major physical, chemical, and biological processes influencing the changes in CO_2 and O_2 concentrations in soils, as shown by different color-coded arrows (Figure 10). The 1:1 ratio line represents the soil respiration process (Rxn (2)), where each consumed O_2 mole generates and releases one mole of CO_2 in accordance with stoichiometry (Gallagher & Breecker, 2020). Soil gas data fall into this line in very biologically active ecosystems (Angert et al., 2015; Hodges et al., 2019; Gallagher & Breecker, 2020).

The green arrow corresponds to the biotic process, which runs parallel to the 1:1 ratio (Rxn (2)). Red arrows indicate major chemical processes (Figure 10). The focus of this study is shown by one red arrow, producing higher abiotic pCO_2 with solid calcite precipitation (Rxn (1)). Particularly, the red arrow directed to the right, indicates increasing CO_2 however O_2 is irrelevant and is independent of available O_2. The second red arrow pointing left likely indicates CO_2 dissolution in water, or potentially CO_2 degassing from soil water (Figure 10). For example, soil CO_2 is always higher concentrations than atmospheric CO_2 (as seen in Figure 6) and when irrigation water is introduced, it attempts to equilibrate with the soil CO_2 concentration therefore CO_2 dissolves in the soil water (forming carbonic acid). This process occurs typically fast, once irrigation water interacts with soil gases (early in an irrigation cycle) and as a result, reduces the pCO_2 levels.

In contrast, the abiotic process requires evaporation to concentrate HCO_3^- and Ca^{2+} in the soil water, driving the precipitation of $CaCO_3$ and the release of abiotic CO_2 gas. This process is

thus expected once the field is no longer saturated with irrigation water and soil moisture levels are significantly lowered (accelerated by evaporation). The last group of important processes modifying the pCO_2 and pO_2 in soil are physical processes. The displacement of gases for incoming irrigation water (purple arrow): once irrigation floods the field, water fills the soil pores, and pushes the gas out of the soil profile, this is important early right after the irrigation, as soon as irrigation floods the field (saturating the soil pores). The other dominant physical process is diffusion (the blue arrow), driven by concentration gradients. The pO_2 is approximately 21% while pCO_2 is about 0.04% in the air. The pO_2 is much lower but the pCO_2 is much higher in the soils (Figures 5 and 6). Thus, O_2 will diffuse into soils while CO_2 will diffuse out of soils towards the atmosphere. This diffusion process is more important later in the irrigation event, as the soil pores have to open up to allow gas diffusion.

Based on the conceptual diagram (Figure 10), pCO_2 and pO_2 data were analyzed for two river water irrigation events: 06/15/2021 - 07/04/2021, lasting 19 days (≈ 3.17 days per color segment), and 07/05/2021 - 07/30/2021, lasting 26 days (≈ 4.3 days per color segment). The analysis was conducted for both Pecan_Coarse (Figure 11) and Pecan_Fine (Figure 12). The examination of these irrigation cycles provides insights into the processes influencing the concentrations of soil CO_2 and O_2; including the impact of precipitation events (refer to Appendix Table 2A).

During the initial irrigation event (06/15/2021 - 07/04/2021) in Pecan_Coarse, a noticeable increase in pCO_2 levels and a decrease in pO_2 levels were observed for the first two days (Figure 11A). This indicates a relatively slower biotic reaction, as the trend deviates slightly from the expected 1:1 ratio line (Figure 10). From day 3 to day 7, the pO_2 and pCO_2 trend closely aligns with the biotic trend in a 1:1 ratio. Between day 7 and day 13, the trend shifts upwards towards

atmospheric conditions, characterized by lower CO_2 concentrations and higher O_2 concentrations, suggesting diffusion with the atmosphere. On day 13, corresponding to a precipitation event on 06/25/2021 with 0.28 inches, the trend is influenced, indicating the rapid dissolution of soil CO_2 gas into the irrigation water (which is in equilibrium with atmospheric CO_2) and displacement of O_2 by water until day 14 (Figure 11A; Appendix Table 2A). From day 15 to day 17, the slope of the trend once again resembles the biotic reaction, with depleted O_2 levels and increasing CO_2 concentrations. During the final two days (18 and 19), the trend continues to be influenced by precipitation, affecting the concentrations of CO_2 and O_2 (Figure 11A; Appendix Table 2A).

During the subsequent irrigation period (07/05/2021-07/31/2021) at Pecan Coarse, on the first day, we observed a depletion of CO2 and O2 concentrations, indicating the anticipated processes of CO_2 dissolution and physical displacement of gases in the soil (Figure 11B). On day 2, the trend exhibited a steeper slope compared to our biotic trend, suggesting a deceleration in biotic CO2 production. On day 3, we once again observed the initial processes of CO2 dissolution and physical displacement of soil gases. By day 4, a trend line almost parallel to the expected biotic 1:1 ratio became apparent. Subsequently, the trend continued in the direction of our diffusion processes until day 17. However, after day 17, a significant rainfall event of 0.69 inches on 07/24/2021 altered the trend's direction (Figure 11B; Appendix Table 2A).

In Pecan_Fine, during the initial irrigation cycle (06/15/2021-07/04/2021) by river water, on the first day, the trend is nearly horizontal, shifting towards the left (indicating decreasing CO_2 concentrations), suggesting CO_2 dissolution into the introduced irrigation water. On day 2, the trend becomes steeper, indicating the physical displacement of soil gases (Figure 12A). By day 3, the trend becomes almost vertical, with decreasing O_2 and some CO_2 production, indicating a biotic trend. However, since the slope deviates from the expected 1:1 ratio, it suggests a potentially

slowed biotic rate. On day 4, the trend becomes nearly parallel to the expected biotic trend, and gradually, by day 5, the trend turns upright, indicating diffusion with biotic CO_2 production until day 6. After day 6, a clear abiotic horizontal trend emerges, moving towards the right until day 13 when precipitation events introduce deviations from the trend. On day 13, a nearly vertical trend is observed, suggesting the dissolution of CO_2 in water (related to the precipitation event on 06/28/2021 of .78 inches), combined with processes maintaining CO_2 concentrations while O_2 is depleted, indicating biotic processes (Appendix Table 2A). From days 17 to 18, an upward trend is observed, indicating the influence of diffusion and biotic CO_2 production, as both O_2 and CO_2 concentrations increase. By day 19, a slow biotic process is observed (Figure 12A).

During the second river irrigation cycle (07/05/2021-07/31/2021) at Pecan_Fine, on day 1, a horizontal trend indicates CO_2 dissolution upon the introduction of irrigation water. This is followed by a physical displacement trend of both gases on day 2. On day 3, a biotic trend with some CO_2 dissolution is observed (Figure 12B). From day 4 to day 7, a positive slope indicates diffusion and biotic processes. For days 8 to day 10, a very shallow, nearly horizontal trend suggests an abiotic trend, producing CO_2. On day 13 (07/18/2021), a small precipitation event of 0.07 inches occurs, potentially changing the trend direction (Appendix Table 2A). From day 13 to day 26, the trend exhibits diffusion, and on day 22 the trend goes above the 1:1 ratio. When comparing the Pecan_Fine and Pecan_Coarse sites, it is noteworthy that the former demonstrates a higher frequency of abiotic trends, while the latter shows trends that more closely resemble the biotic trend (Figure 11 and Figure 12).

After the pecan orchard is flood irrigated, there is a decrease in the concentration of soil CO_2 gas as well as O_2 gas. However, this decrease is not solely attributed to the physical displacement caused by the irrigation events, as there are instances where the decline in CO_2

concentration occurs after a production peak in the soil (Figures 6A and 6B). This decrease is observed in the falling limbs of the concentration curves indicating the rate of consumption or diffusion is greater than the rate of CO_2 production. In an irrigated system, time is a critical factor in maintaining optimal CO_2 concentrations in the soil. Moisture occupying soil pores does not directly affect CO_2 concentration. Instead, it allows chemical reactions to take place, which affect the soil concentrations by either producing or consuming CO_2. A similarity to O_2 when comparing both irrigated sites is that trends for 30 and 60 cm are closer in values at Pecan_Coarse (Figure 5A and B), indicating that the depth is not as crucial in coarser soil textures as it is in finer ones.

In general, we can compare the observed patterns for both soil textures by analyzing two consecutive Rio Grande irrigations (depicted in Figures 11 and 12). At Pecan_Coarse, we do not observe the initial processes occurring at Pecan_Fine, where CO_2 dissolves into the irrigation water (resulting in a decrease in CO_2) and soil gases are physically displaced. Instead, we observe more biotic trends responding after irrigation. Additionally, we notice that in Pecan_Fine, when the soil becomes dry, abiotic trends are more apparent compared to Pecan_Coarse. Another way to visually interpret the time series within irrigation cycles is to draw a line across the entire dataset representing its average trend. From this, we can infer that abiotic CO_2 is the dominant process in Pecan_Fine, while biotic CO_2 is the dominant process at Pecan_Coarse.

6.4 Co-evolution of pCO2 vs pO2 in a Natural Dryland System

At our natural site located within the Jornada experimental range (JER_VM), 145 days (08/27/2021 – 04/01/2021) of pCO_2 and pO_2 data are recorded for 15 and 30 cm respectively with each color-coded segment representing ≈ 24 days (Figure 13). While the natural system exhibits less dynamism compared to our irrigated system, it presents interesting diurnal variability in soil

moisture, O_2, and CO_2, providing opportunities for interpretation (refer to Appendix Figure 2). Overall, we observe a trend in CO_2 and O_2 concentrations that resembles biotic activity, showing parallelism to the 1:1 ratio. Notably, during the fall season, CO_2 values exhibit larger ranges, ranging approximately from 0.05% to 0.18%. In contrast, during the winter and early spring, CO_2 levels are lower, typically ranging from 0.04% to 0.08% (Figure 13), accompanied by slightly higher O_2 levels (Figure 6C). The observed increase in CO_2 levels during late summer and early fall can be attributed to the activation of biotic processes in the soil stimulated by the monsoon season and warmer temperatures. Conversely, the decrease in precipitation and colder temperatures during winter and early spring limit biotic CO_2 production (Figure 6C).

7. CONCLUSIONS

In natural dryland ecosystems, water availability is controlled by limited precipitation. However, in agricultural areas, irrigation is used, and with its high salinity, leads to salt accumulation in soils and enhances the precipitation of pedogenic carbonates through the process of evapotranspiration thus releasing abiotic CO_2. Irrigation practices also promote soil respiration, releasing biotic CO_2 although water saturation could limit oxygen O_2 availability and reduce the rates during wetter periods.

Soil texture plays a crucial role in regulating moisture content and gas concentrations in soils. At the Pecan_Fine site with a finer texture, soils have limited fluid mobility, different from those at the Pecan_Coarse site. Indeed, water retention is higher in Pecan_Fine compared to Pecan_Coarse due to differences in infiltration rates. Furthermore, O_2 and CO_2 concentrations at Pecan_Coarse decrease after irrigation and precipitation events, albeit not as significantly as in Pecan_Fine, where greater depletion is observed. Additionally, peak concentrations of CO_2 at Pecan_Coarse occur earlier (within the first 10 days) during irrigation cycles, while peak concentrations at Pecan_Fine are reached later (after 10 days). In the natural dryland control site, JER_VM, we observe more stable fluctuations in fluid mobility and resulting concentrations. However, precipitation events increase both soil moisture and O_2 concentrations, while CO_2 concentrations show a slight increase after such sporadic events.

In order to distinguish between soil-respired CO_2 and abiotic calcite-derived CO_2, $\delta^{13}C$ of soil gas samples are utilized after estimating the isotope ratios of different end-members. Through a two-component mixing equation, we determined that the abiotic process accounted for 61-72% of total soil CO_2 at the Pecan_Fine site, but only 42-47% at the Pecan_Coarse site when using groundwater as the irrigation source. During river water irrigations, Pecan_Fine contributed 35-

37% of abiotic CO_2, while Pecan_Coarse contributed 24-27%. These results highlight the critical role of irrigation water chemistry in determining the source of CO_2 production with respect to differing soil textures. For the year 2021, we are confident about the relative abiotic CO_2 contributions for the first irrigation sampled, as it was the initial source for the first three irrigations. However, abiotic contributions for gas samples collected during river water irrigation are likely with a large error bar, due to the legacy of groundwater in the soils. This remaining soil water can mix with the river water, affecting the C isotope signatures of our abiotic CO_2 calculations.

The high resolution of CO_2 and O_2 concentrations in the soil allowed us to examine specific processes after each irrigation. Upon irrigating the field, we observed initial water-soil gas interactions, namely, the chemical dissolution of soil CO_2 into the irrigation water, resulting in a reduction in soil CO_2 levels. When water infiltrates the soil, lowering O_2, we can expect reduced soil respiration and thus limited biotic CO_2 production. Indeed, at the Pecan_Fine site, where soil saturation can last up to approximately 5 days, soil conditions become anoxic, and soil respiration is probably minimum. Higher evaporation intensified by the high temperatures typical of arid environments in the summer drives the abiotic reaction to the right, leading to the supersaturation of ionic compounds and subsequent precipitation of salts, including pedogenic carbonate, and the release of abiotic CO_2 in the soil. As moisture decreases due to infiltration or evapotranspiration, diffusion becomes faster for gases between soil and the atmosphere, lowering soil CO_2 and increasing O_2. This will increase the soil respiration rates too, releasing more soil-respired CO_2.

The outcomes of this research have the potential to provide valuable insights into the role of soil CO_2 in the carbon cycle of irrigated drylands. With the work of this research, we can interpret how soil textures and water chemistry potentially affect the abiotic and biotic processes

responsible for fluctuations in soil gases (CO_2, and O_2) and differentiate these processes. Further research in this area may contribute to our understanding of the impacts of irrigation practices on carbon dynamics in agricultural ecosystems and aid in the development of sustainable agricultural management strategies.

8. FUTURE DIRECTIONS

Research has the potential to expand the scope of this project by investigating spatial and temporal variations in different study areas and over multiple irrigation seasons. Further expansion of this study could involve collecting additional soil gas samples from natural dryland areas, as well as a larger quantity of irrigation water samples, to compare with previous studies. Despite the installation of lysimeters at Pecan_Coarse and Pecan_Fine, the collection of soil water after flood irrigation events were not performed effectively, unfortunately. This missed opportunity could have provided a valuable source for water chemical analyses. Future investigations could also focus on diurnal variabilities, examining daily fluctuations of CO_2 concentrations as a function of temperature in natural and irrigated sites. Pressure differences between the atmosphere and soil at various depths could provide insights into the role of advection in soil gas concentrations and circulation patterns. Water isotopic data, particularly $\delta^{18}O$, could be useful for understanding potential correlations between isotopic signatures and gas concentrations in the soil. Additionally, the impact of amendments used in pecan orchards, such as nutrients and tillage practices, on soil gas concentrations and reactions could be an interesting factor to consider. Furthermore, biological aspects, including the role of plants and microorganisms, as indicators of gas concentrations and processes in the soil, should be taken into account in future studies.

Table 1: Describes all sensors that were used for this collaborative research project, at the three study sites within two locations (study areas).

Sensor	Data Measured	Data Collection	Location	Study Site	Depths
ECH$_2$O 5TE (METER)	Volumetric Water Content (VWC)	CR1000 Data logger (Campbell Scientific)	Pecan_Orchard	Pecan_Fine/ Pecan_Coarse	30, 60$^+$ cm
TEROS 12 (METER)	Volumetric Water Content (VWC)	METER ZL6 Data logger (Zentra Cloud)	Pecan_Orchard	Pecan_Fine/ Pecan_Coarse	90, 120, 150* cm
CS650 (Campbell Scientific)	Volumetric Water Content (VWC)	CR1000 data logger (Campbell Scientific)	Jornada Experimental Range	JER_VM	15, 30 cm
eosGPCO_2 (Eosense)	Carbon dioxide (CO_2) concentrations	CR1000 Data logger (Campbell Scientific)	Pecan_Orchard	Pecan_Fine/ Pecan_Coarse	30, 60 cm
			Jornada Experimental Range	JER_VM	15, 30 cm
Oxygen Sensor SO-110 (Apogee)	Oxygen (O_2) concentrations	CR1000 Data logger (Campbell Scientific)	Pecan_Orchard	Pecan_Fine/ Pecan_Coarse	30, 60 cm
			Jornada Experimental Range	JER_VM	15, 30 cm[1]

*150 cm TEROS 12 is not functional at Pecan_Fine.

+ Due to a power issue, ECH2O 5TE data were not recorded during 08/14/2021 – 10/19/2021 at Pecan_Coarse.

Table 2: A) Shows the statistical values for R_{mix} (‰, ±) and X_A (‰, ±) that were calculated for groundwater samples (06/08/2021 – 06/15/2021), B) shows the same statistical values but for the river water samples (06/24/2021 – 08/26/2021). The columns specify Pecan_Coarse or Pecan_Fine sites with contrasting soil textures at 60 and 100 cm and the number of gas samples (n) pertaining to each group.

A. Groundwater	Pecan_ Coarse_60 (n=10)	Pecan_Coarse_100 (n=10)	Pecan_Fine_60 (n=10)	Pecan_Fine_100 (n=10)
R_{mix} (‰)	-21.36	-21.72	-20.41	-19.68
R_{mix} ±	0.41	0.48	0.28	0.13
X_A (%)	47	42	61	72
X_A ±	6	7	4	2

B. River water	Pecan_ Coarse_60 (n=9)	Pecan_Coarse_100 (n=9)	Pecan_Fine_60 (n=9)	Pecan_Fine_100 (n=9)
R_{mix} (‰)	-21.68	-21.37	-20.42	-20.18
R_{mix} ±	0.43	0.34	0.44	0.42
X_A (%)	24	27	35	37
X_A ±	4	3	4	4

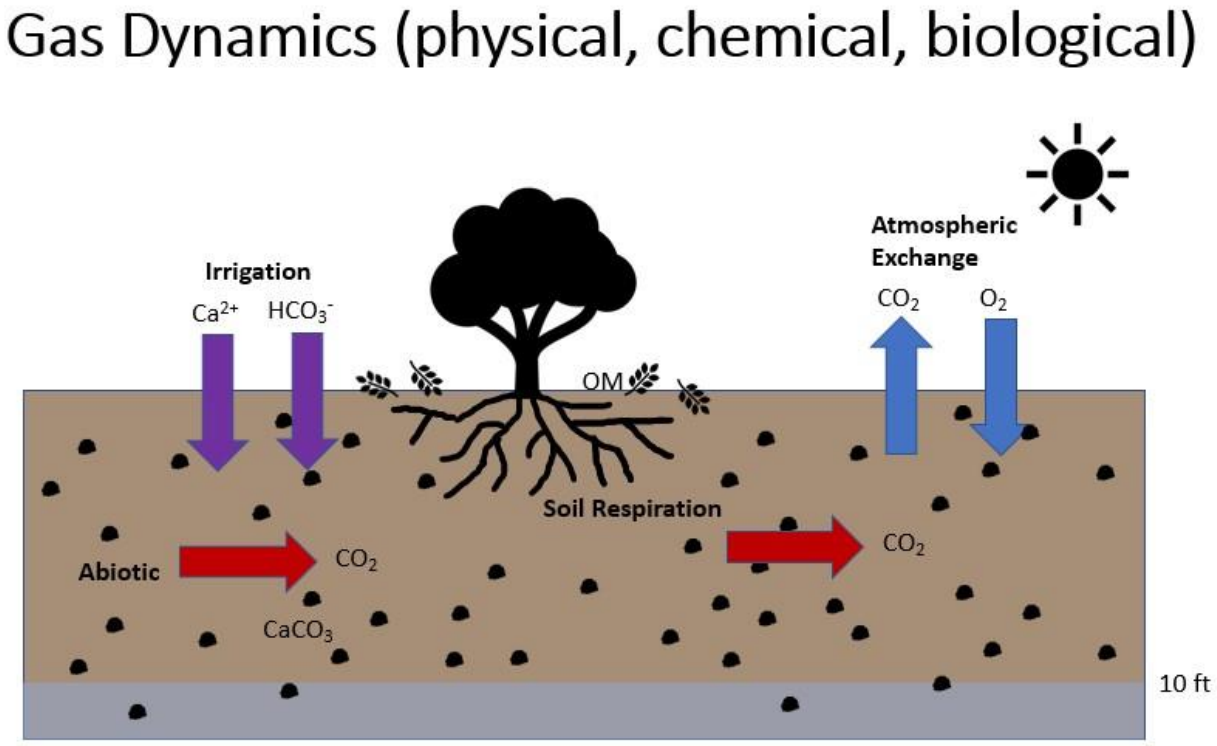

Figure 1: Diagram showing gas dynamics investigated, precipitation of pedogenic carbonate ($CaCO_3$), soil respiration, atmospheric exchange, and ions supplied by irrigation water (precipitation). Both abiotic (precipitation of pedogenic carbonate) and biotic (soil respiration) processes produce CO_2 in the soil.

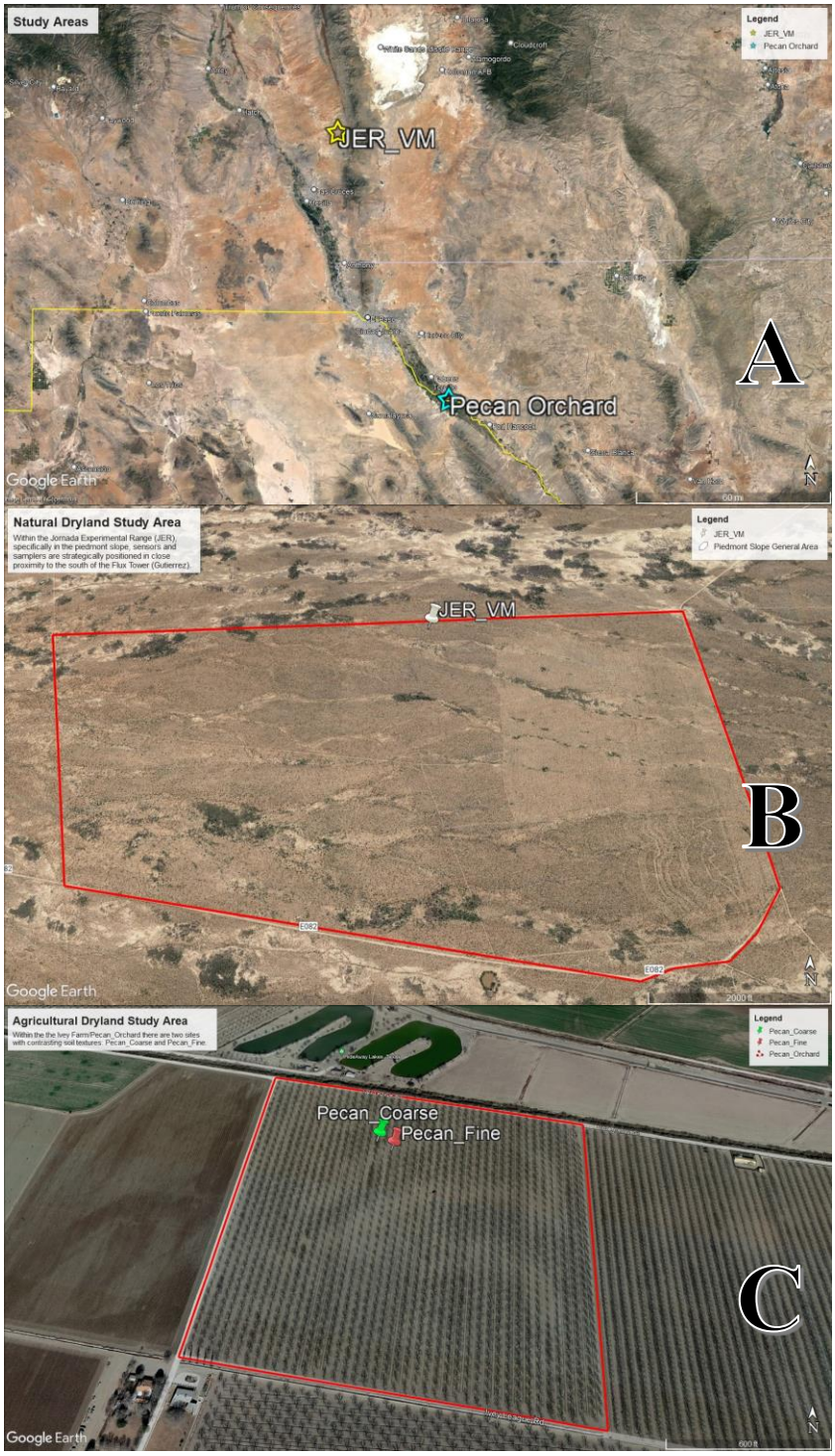

Figure 2: A) Regional map that pinpoints the study locations, the cyan star depicts where the pecan orchard is located in Texas, and the yellow star indicate where the piedmont slope in the Jornada - Experimental Range (JER_VM) is located in New Mexico. Study Sites are all within dryland in the Rio Grande Basin, Chihuahuan desert. B) Large-scale map outlining our natural study area in red (JER_VM). The general area is within a piedmont slope location within the Jornada Experimental Range, the actual site of the collection is near Gutierrez's flux tower. C) Large-scale map outlining our agricultural study area in red (pecan orchard). Lighter segments in the pecan field are segments where trees are smaller (Pecan_Fine), and darker areas have larger trees (Pecan_Coarse).

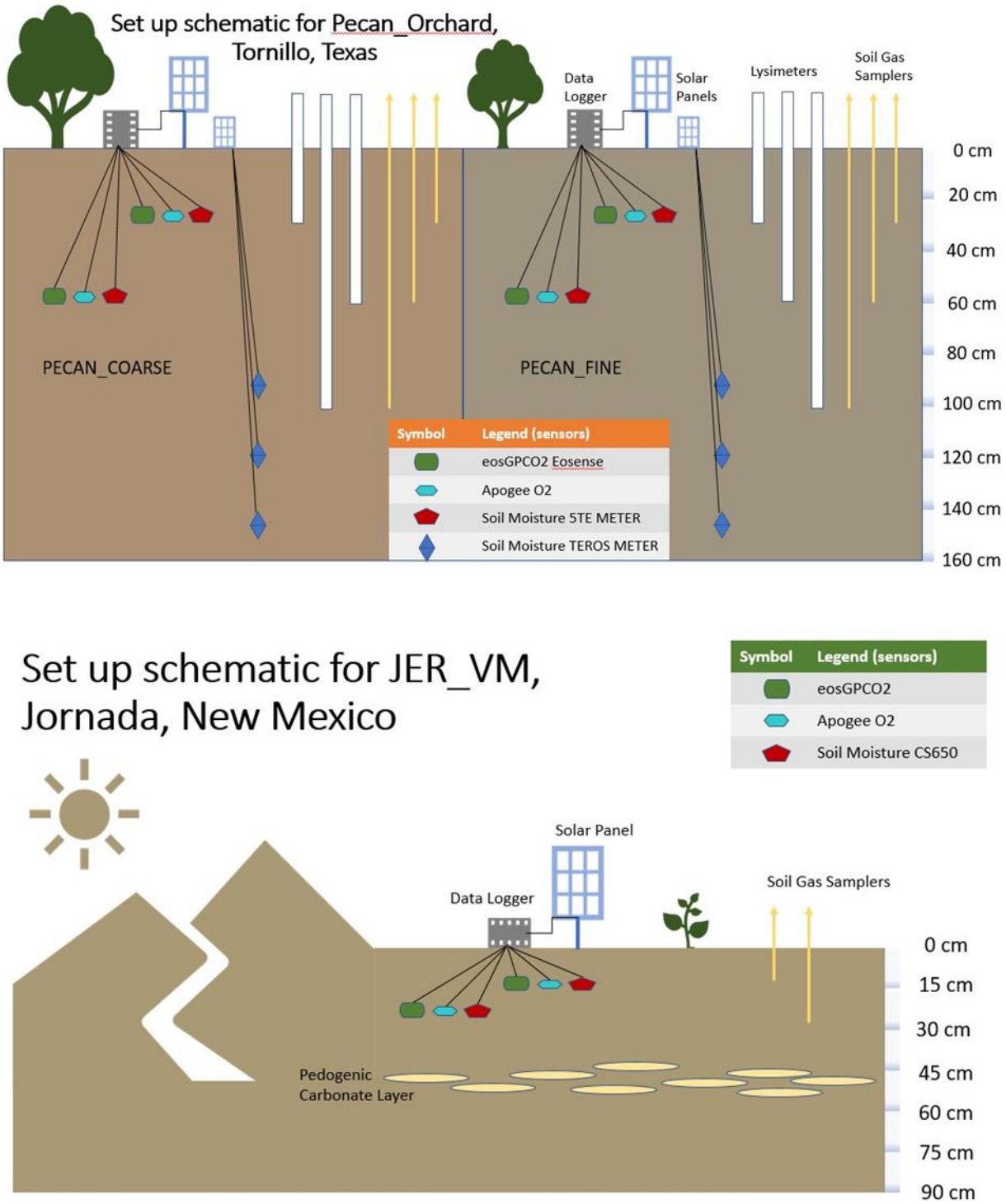

Figure 3: A set-up schematic for the pecan orchard study sites (A) and the JER_VM site (B) illustrating the setup and placement of sensors and gas samplers at depth.

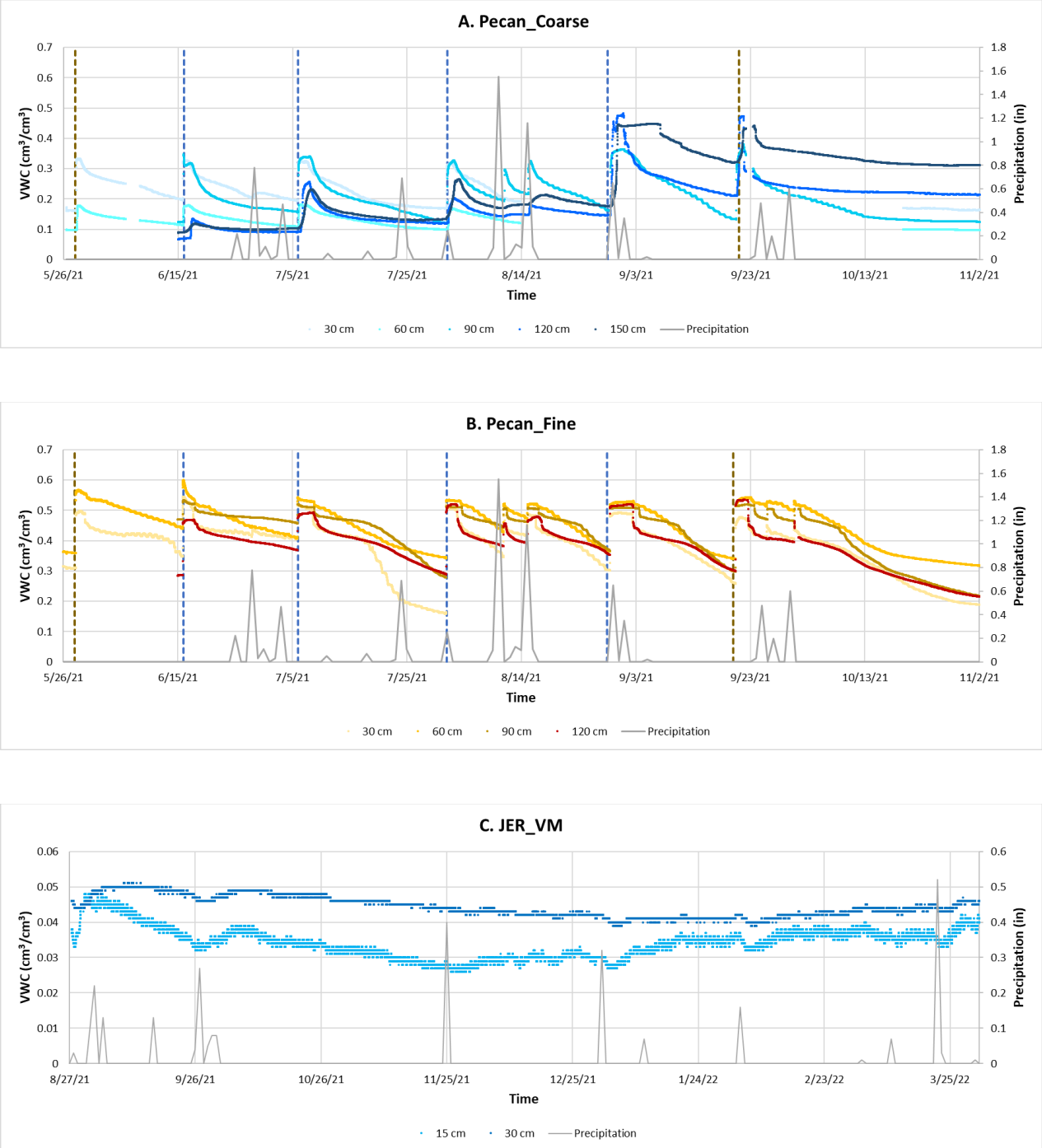

Figure 4: Variation of volumetric water content (VWC) at the A) Pecan_Coarse and B) Pecan_Fine study sites, as a function of irrigation and precipitation events in 2021. Precipitation data are from NOAA (Station: TORNILLO 2 SSE, TX US). The vertical dashed lines represent the flood irrigation events (brown lines indicate irrigation by groundwater and blue by river water). C) Volumetric Water Content (VWC) recorded by sensors at the natural JER_VM study site, includes precipitation data from NOAA (Station: JORNADA EXPERIMENTAL RANGE, NM US).

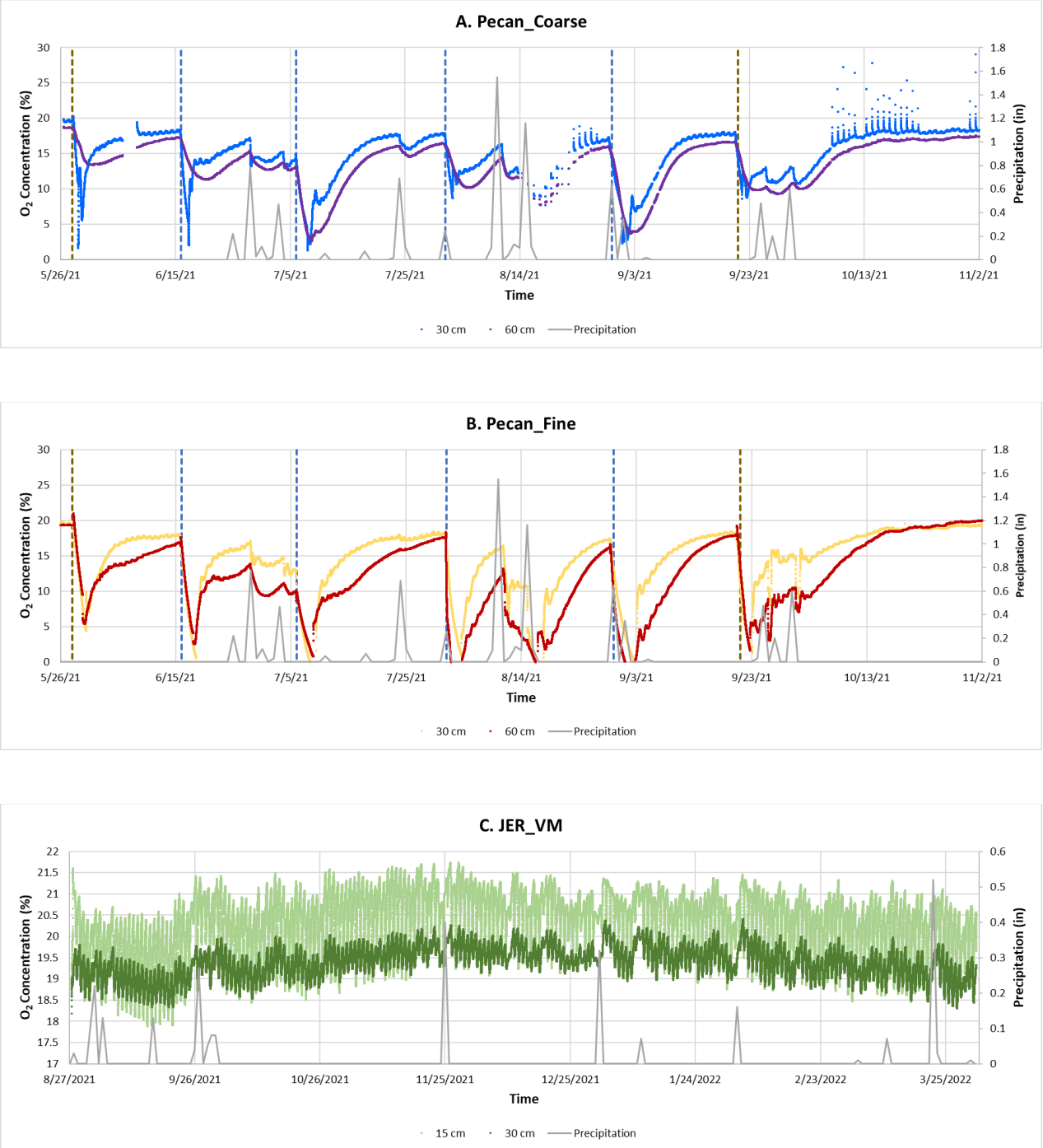

Figure 5: Soil O_2 time series for A) Pecan_Coarse and B) Pecan_Fine site, including irrigation events and precipitation data from NOAA (station: TORNILLO 2 SSE, TX US). Flood Irrigations are shown as vertical dashed lines; brown indicates groundwater while blue indicates river water. C) Soil O_2 time series for JER_VM site, including precipitation data from NOAA (Station: JORNADA EXPERIMENTAL RANGE, NM US). O_2 sensor data (scatterplot) is plotted on the primary y-axis while recorded precipitation (bar plot) is plotted on the secondary y-axis.

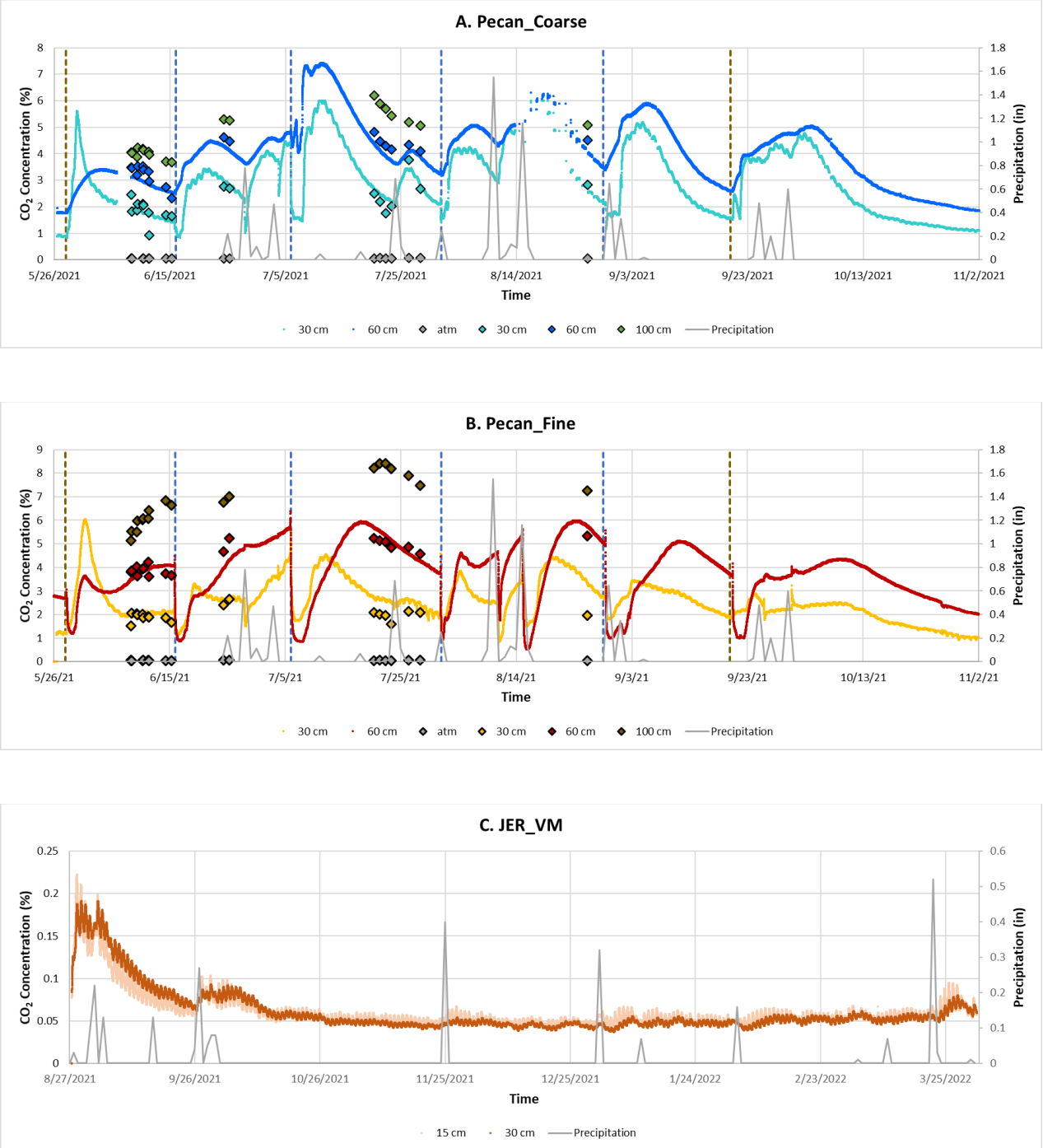

Figure 6: CO_2 time series for A) Pecan_Fine and B) Pecan_Coarse sites, including irrigation events and precipitation data from NOAA (station: TORNILLO 2 SSE, TX US). Flood Irrigations are shown as vertical dashed lines; brown indicates groundwater while blue indicates river water. C) Soil CO_2 time series for JER_VM site, including precipitation data from NOAA (Station: JORNADA EXPERIMENTAL RANGE, NM US). CO_2 sensor data (scatterplot) is plotted on the primary y-axis with convenience CO_2 gas samples analyzed at UC Davis, while recorded precipitation (bar plot) is plotted on the secondary y-axis.

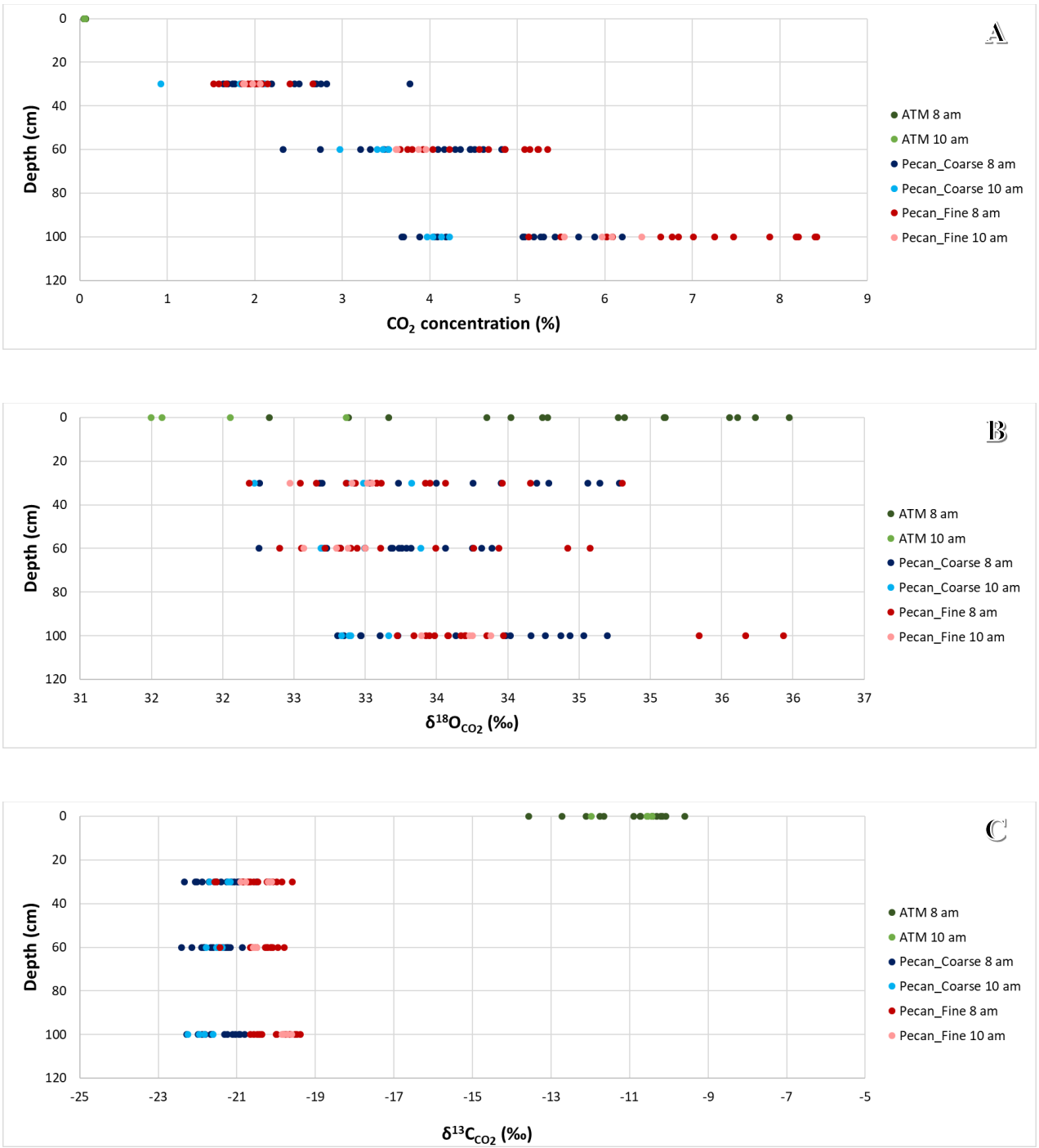

Figure 7: Soil gas concentrations; A) CO_2 depth plot showing diffusion curve, B) $\delta^{13}C$ depth plot and C) $\delta 1^{8}O$ depth plot, specifying site (Pecan_Coarse and Pecan_Fine) and time of sampling (10 a.m. or 8 a.m.). Green dots represent atmospheric gas samples, blue dots represent Pecan_Coarse, and red dots represent Pecan_Fine, the darkness of color specifies the time of sampling.

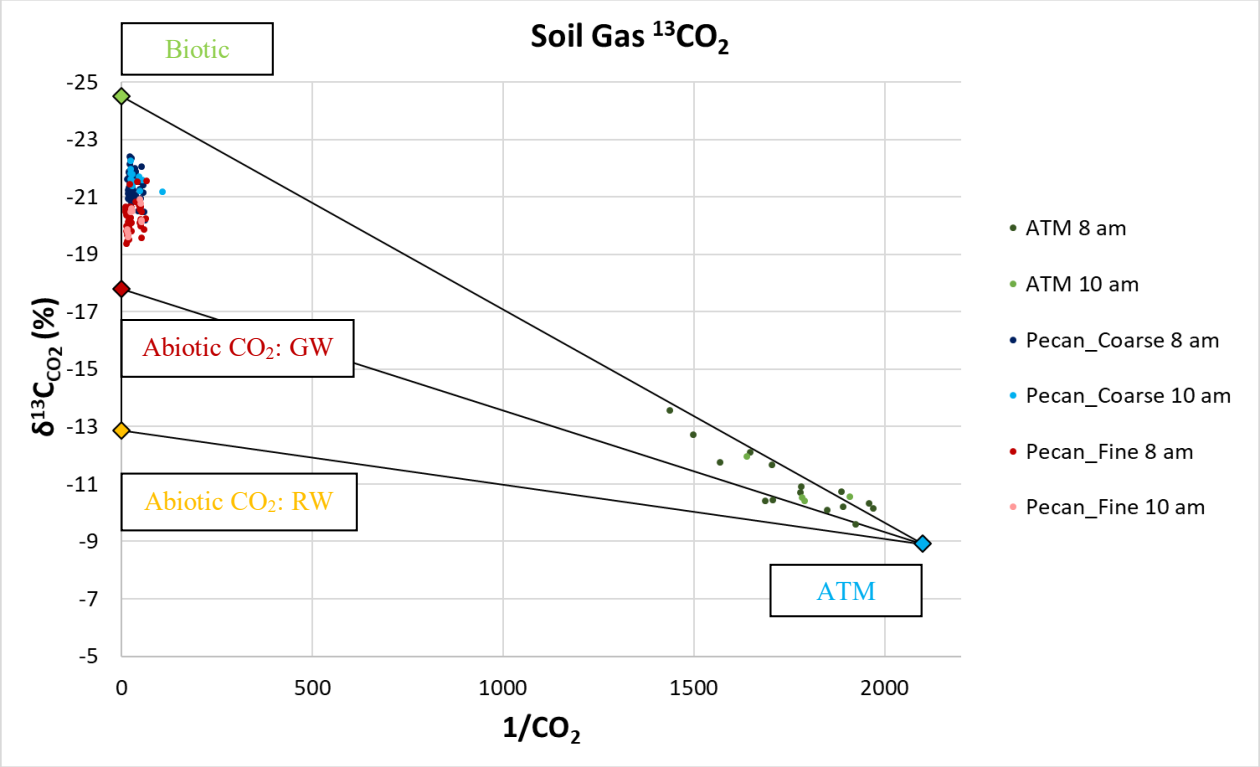

Figure 8: Keeling plot showing contributing sources for CO_2 based on $\delta^{13}C$ soil gas samples. There are four CO_2 endmembers and their mixing lines: atmospheric (ATM), biotic, abiotic groundwater (GW), and abiotic (RW).

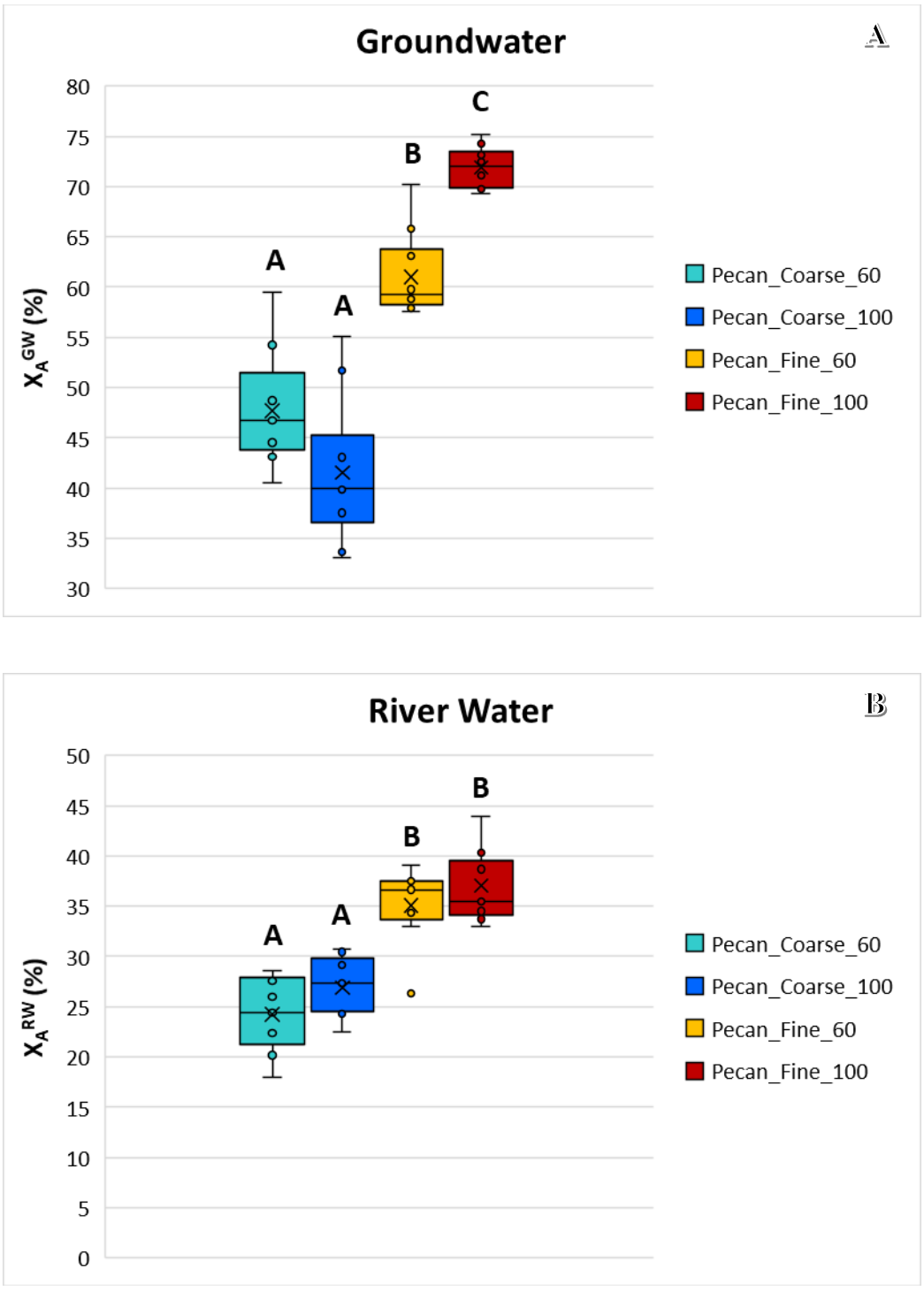

Figure 9: X_A box plots indicating mean and standard deviations with outliners, letters A, and B above boxes are used for grouping based on significance difference ($p < 0.05$). A) Is regarding Groundwater values, while B) is regarding river water values.

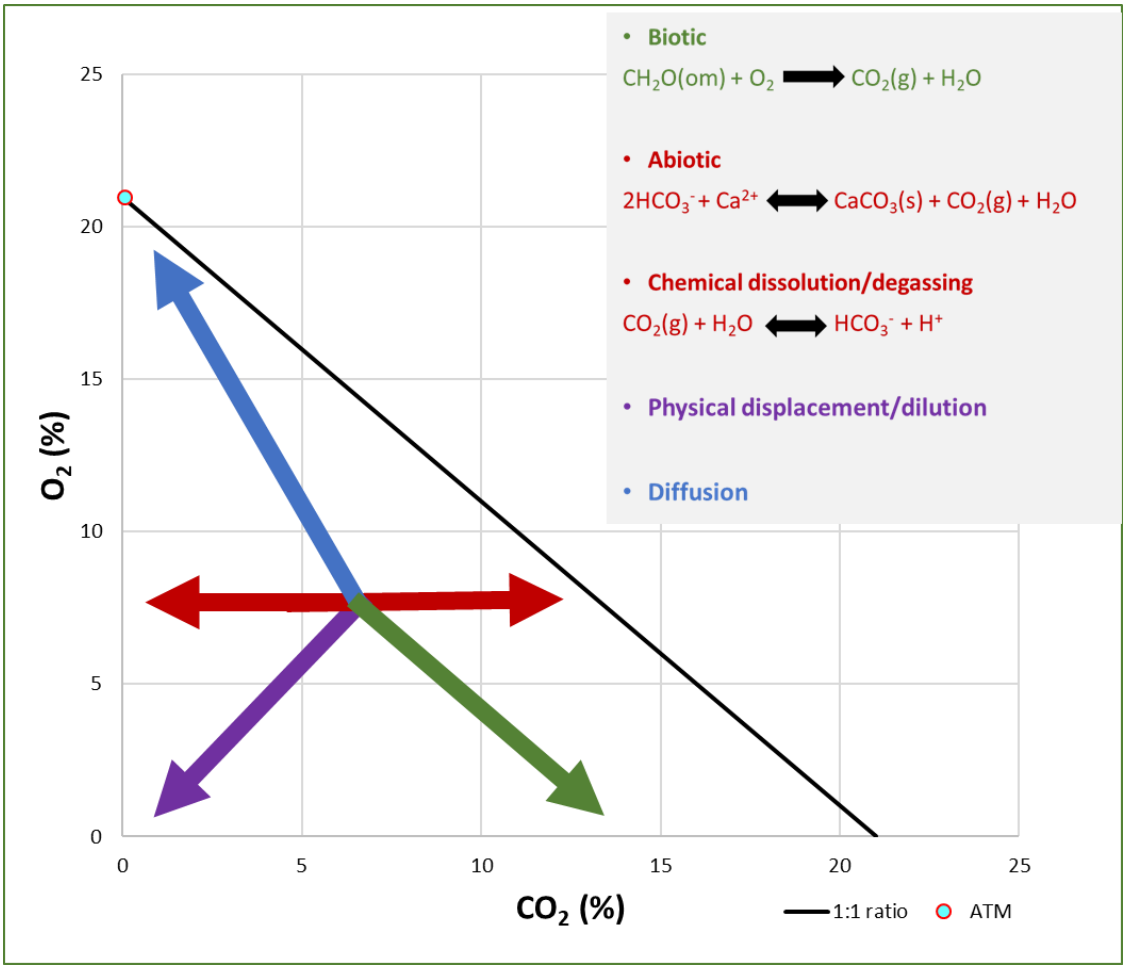

Figure 10: Depicts various dominating processes affecting congruently the CO_2 and O_2 concentrations, we include the 1:1 ratio representing our biotic reaction processes (black line), and the atmospheric concentrations (cyan dot with red outline).

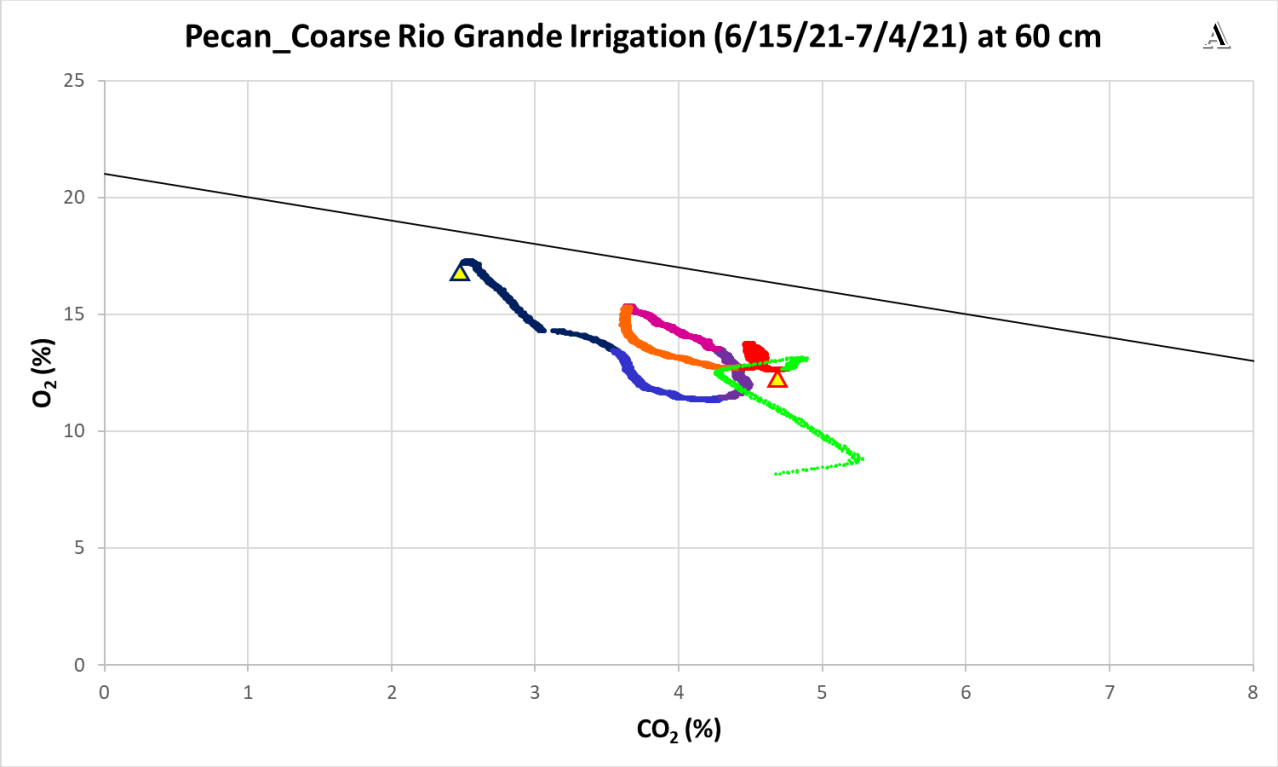

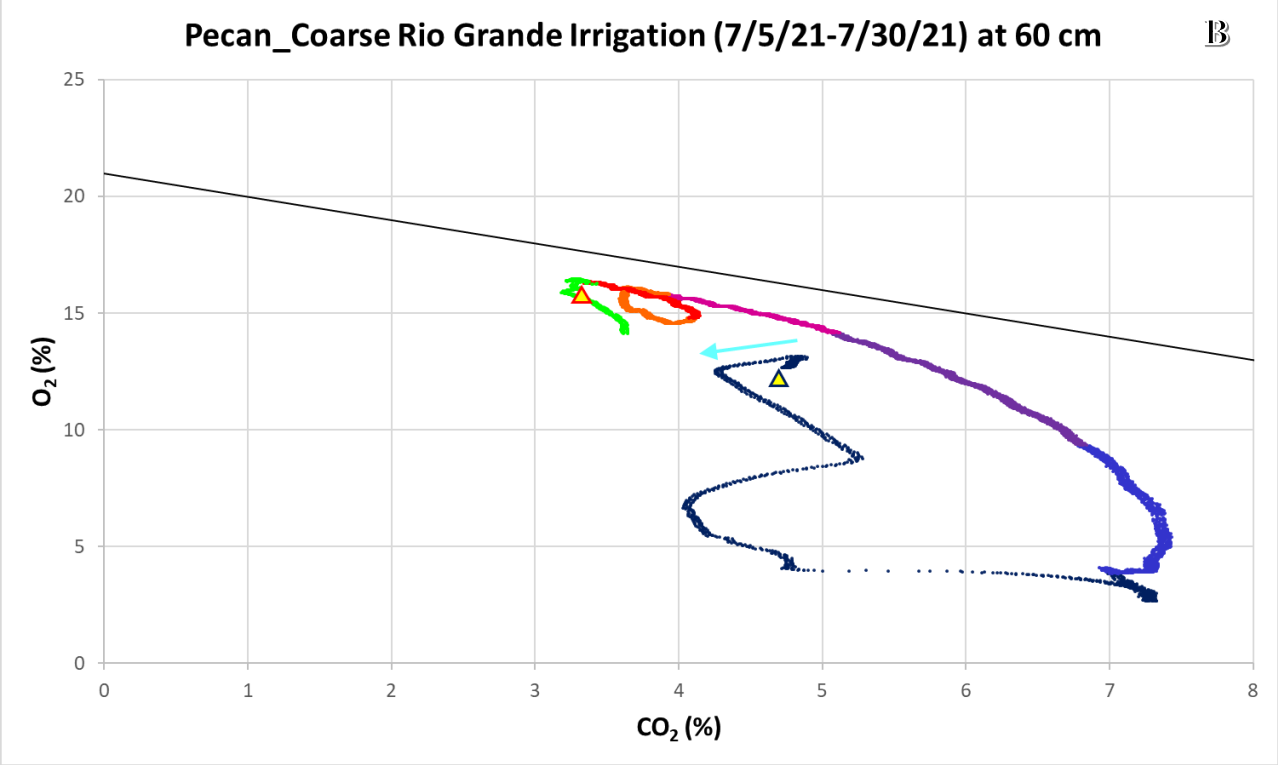

Figure 11: Pecan_Coarse CO_2 and O_2 at 60 cm coevolution trend shown for an irrigation cycle (IRW-RG1 and IRW-RG2). A) IRW-RG1 is from 06/15/2021-07/04/2021, and B) IRW-RG2 is from 07/05/2021-07/31/2021.

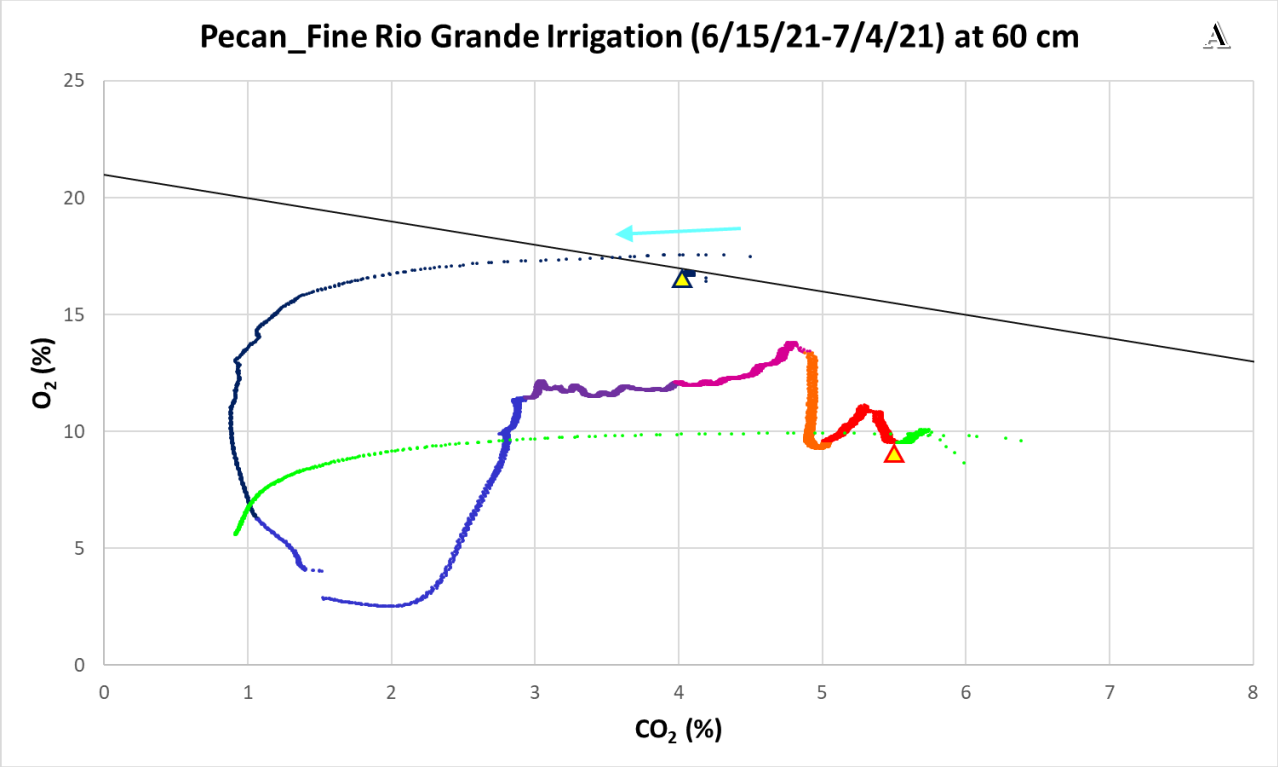

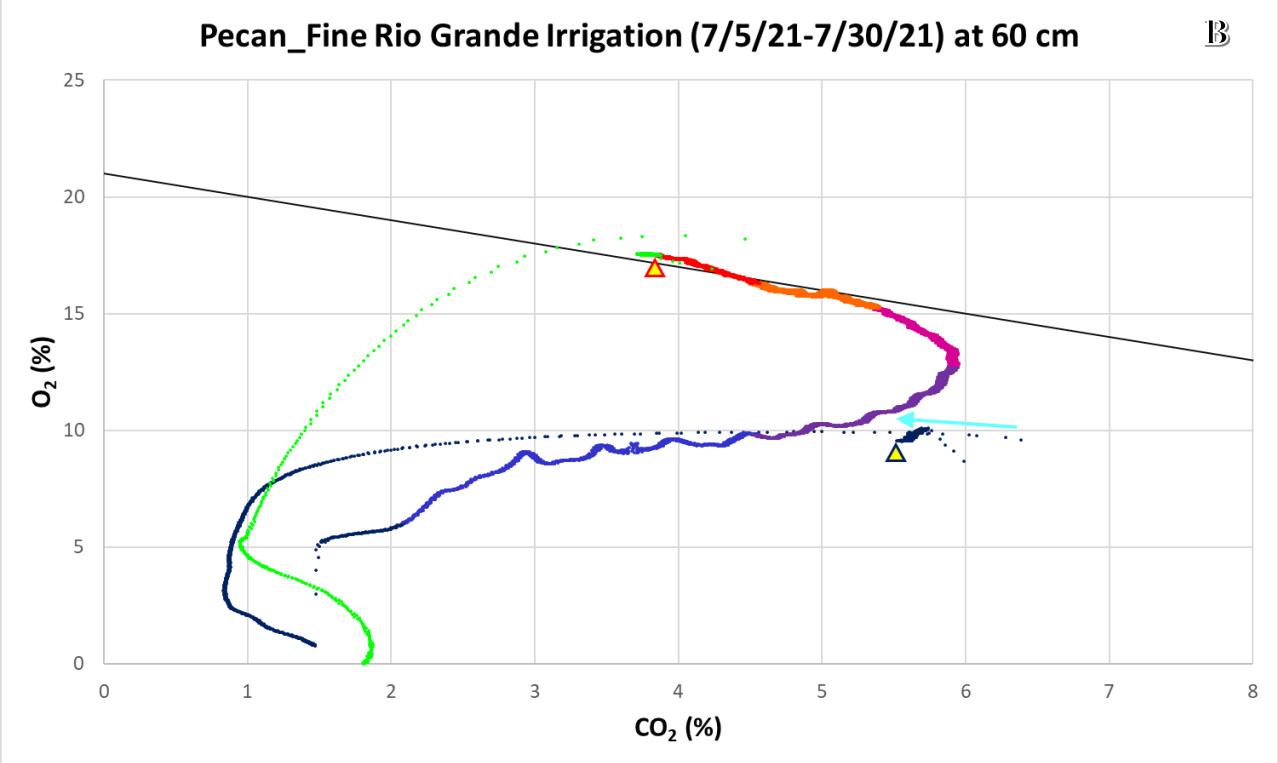

Figure 12: Pecan_Fine CO_2 and O_2 at 60 cm coevolution trend shown for an irrigation cycle (IRW-RG1 and IRW-RG2). A) IRW-RG1 is from 06/15/2021-07/04/2021, and B) IRW-RG2 is from 07/05/2021-07/31/2021.

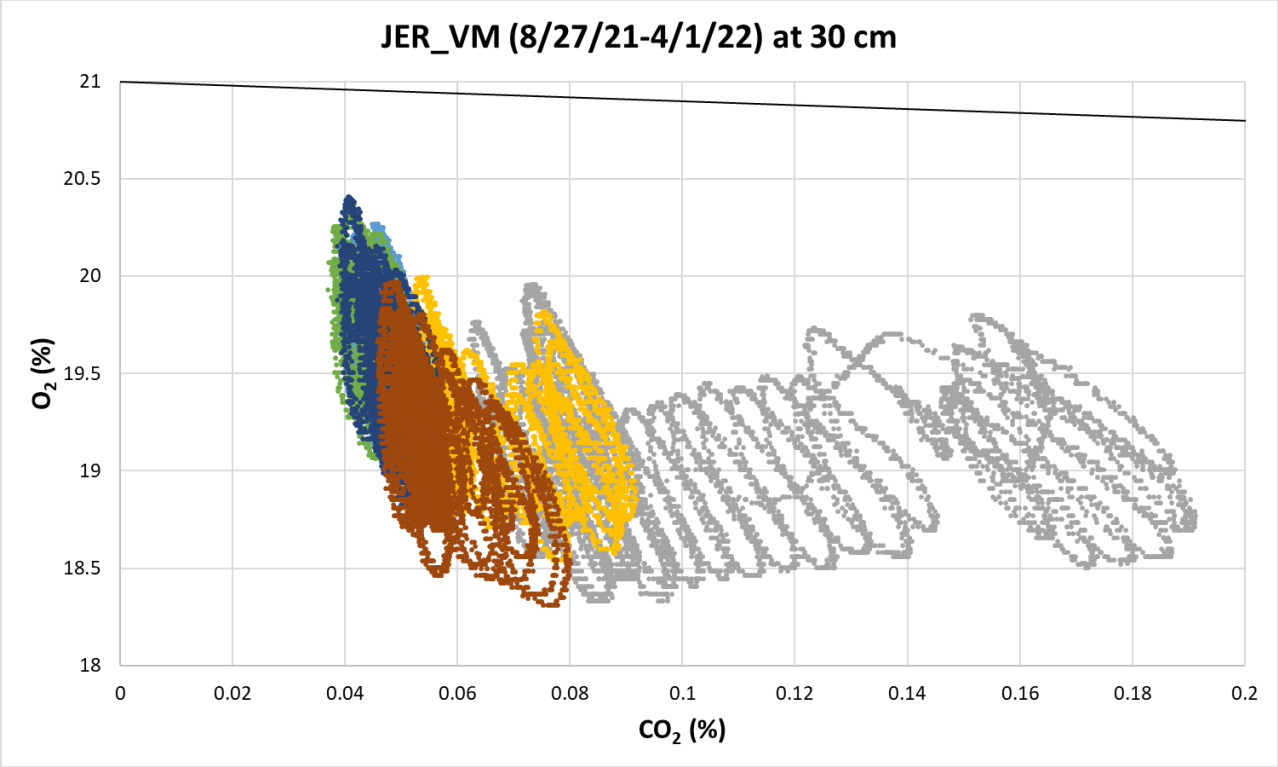

Figure 13: JER_VM CO_2 and O_2 at 30 cm coevolution trend from 08/27/2021 – 04/01/2021. The general direction of the trend is moving from right to left.

9. REFERENCES

Angert, A., Yakir, D., Rodeghiero, M., Preisler, Y., Davidson, E. A., & Weiner, T. (2015). Using O2 to study the relationships between soil CO2 efflux and soil respiration. *Biogeosciences*, *12*(7), 2089–2099. https://doi.org/10.5194/bg-12-2089-2015

Clark, I. D., & Fritz, P. (1997). *Environmental isotopes in hydrogeology*. CRC Press/Lewis Publishers.

Cox, C., Jin, L., Ganjegunte, G., Borrok, D., Lougheed, V., & Ma, L. (2018). Soil quality changes due to flood irrigation in agricultural fields along the Rio Grande in western Texas. *Applied Geochemistry*, *90*, 87–100. https://doi.org/10.1016/j.apgeochem.2017.12.019

Doser, D. I., Ornelas, M. A., Martinez, I., Jin, L., Ortiz, A., & Kaip, G. M. (2019). Using Geophysics to Investigate Texture and Salinity of Agricultural Soils and Their Impact on Crop Growth in El Paso County, Texas. *Journal of Environmental and Engineering Geophysics*, *24*(3), 465–477. https://doi.org/10.2113/JEEG24.3.465

Durand, N., Monger, H. C., Canti, M. G., & Verrecchia, E. P. (2018). Calcium Carbonate Features. In *Interpretation of Micromorphological Features of Soils and Regoliths* (pp. 205–258). Elsevier. https://doi.org/10.1016/B978-0-444-63522-8.00009-7

Ezcurra, E., & United Nations Environment Programme (Eds.). (2006). *Global deserts outlook*. Division of Early Warning and Assessment, United Nations Environment Programme.

Gallagher, T. M., & Breecker, D. O. (2020). The Obscuring Effects of Calcite Dissolution and Formation on Quantifying Soil Respiration. *Global Biogeochemical Cycles*, *34*(12). https://doi.org/10.1029/2020GB006584

Ganjegunte, G. K., & Braun, R. J. (2011). Delineating Salinity and Sodicity Distribution in Major Soil Map Units of El Paso, Texas, Using Electromagnetic Induction Technique. *Soil Science*, *176*(8), 441–447. https://doi.org/10.1097/SS.0b013e318221f11a

Gardea, M. E. (2022). *WATER SOURCING STRATEGIES OF DESERT VEGETATION IN VARYING SOIL TEXTURES WITH VEGETATION COMPETITION: A STABLE ISOTOPE ANALYSIS*.

Gocke, M., Pustovoytov, K., Kühn, P., Wiesenberg, G. L. B., Löscher, M., & Kuzyakov, Y. (2011). Carbonate rhizoliths in loess and their implications for paleoenvironmental reconstruction revealed by isotopic composition: Δ13C, 14C. *Chemical Geology*, *283*(3–4), 251–260. https://doi.org/10.1016/j.chemgeo.2011.01.022

Hannam, K. D., Midwood, A. J., Neilsen, D., Forge, T. A., & Jones, M. D. (2019). Bicarbonates dissolved in irrigation water contribute to soil CO2 efflux. *Geoderma*, *337*, 1097–1104. https://doi.org/10.1016/j.geoderma.2018.10.040

Hasenmueller, E. A., Jin, L., Stinchcomb, G. E., Lin, H., Brantley, S. L., & Kaye, J. P. (2015). Topographic controls on the depth distribution of soil CO2 in a small temperate watershed. *Applied Geochemistry*, *63*, 58–69. https://doi.org/10.1016/j.apgeochem.2015.07.005

Hilhorst, M. A. (2000). A Pore Water Conductivity Sensor. *Soil Science Society of America Journal*, *64*(6), 1922–1925. https://doi.org/10.2136/sssaj2000.6461922x

Hillel, D. (1980). *Applications of Soil Physics*. Elsevier.

Hodges, C., Kim, H., Brantley, S. L., & Kaye, J. (2019). Soil CO_2 and O_2 Concentrations Illuminate the Relative Importance of Weathering and Respiration to Seasonal Soil Gas

Fluctuations. *Soil Science Society of America Journal*, *83*(4), 1167–1180. https://doi.org/10.2136/sssaj2019.02.0049

Jin, L., Ogrinc, N., Yesavage, T., Hasenmueller, E. A., Ma, L., Sullivan, P. L., Kaye, J., Duffy, C., & Brantley, S. L. (2014). The CO 2 consumption potential during gray shale weathering: Insights from the evolution of carbon isotopes in the Susquehanna Shale Hills critical zone observatory. *Geochimica et Cosmochimica Acta*, *142*, 260–280. https://doi.org/10.1016/j.gca.2014.07.006

Kramer, P. J., & Boyer, J. S. (1995). *Water Relations of Plants and Soils*. Academic Press.

Laity, J. (2008). *Deserts and Desert Environments*. John Wiley & Sons.

Liu, J., Fa, K., Zhang, Y., Wu, B., Qin, S., & Jia, X. (2015). Abiotic CO_2 uptake from the atmosphere by semiarid desert soil and its partitioning into soil phases: ABIOTIC CO_2 ABSORPTION. *Geophysical Research Letters*, *42*(14), 5779–5785. https://doi.org/10.1002/2015GL064689

Miyamoto, S., Riley, T., Gobran, G., & Petticrew, J. (1986). Effects of saline water irrigation on soil salinity, Pecan tree growth and nut production. *Irrigation Science*, *7*(2). https://doi.org/10.1007/BF00259425

Muscolo, A., Sidari, M., Panuccio, M. R., Santonoceto, C., Orsini, F., & Pascale, S. D. (2011). *Plant Responses in Saline and Arid Environments: An Overview*. *2*, 11.

Naorem, A., Jayaraman, S., Dalal, R. C., Patra, A., Rao, C. S., & Lal, R. (2022). Soil Inorganic Carbon as a Potential Sink in Carbon Storage in Dryland Soils—A Review. *Agriculture*, *12*(8), 1256. https://doi.org/10.3390/agriculture12081256

Nyachoti, S., Jin, L., Tweedie, C. E., & Ma, L. (2019). Insight into factors controlling formation rates of pedogenic carbonates: A combined geochemical and isotopic approach in dryland

soils of the US Southwest. *Chemical Geology*, *527*, 118503. https://doi.org/10.1016/j.chemgeo.2017.10.014

Ortiz, A. C., & Jin, L. (2021). Chemical and hydrological controls on salt accumulation in irrigated soils of southwestern U.S. *Geoderma*, *391*, 114976. https://doi.org/10.1016/j.geoderma.2021.114976

Ortiz, A. C., Jin, L., Ogrinc, N., Kaye, J., Krajnc, B., & Ma, L. (2022). Dryland irrigation increases accumulation rates of pedogenic carbonate and releases soil abiotic CO2. *Scientific Reports*, *12*(1), 464. https://doi.org/10.1038/s41598-021-04226-3

Plaza, C., Zaccone, C., Sawicka, K., Méndez, A. M., Tarquis, A., Gascó, G., Heuvelink, G. B. M., Schuur, E. A. G., & Maestre, F. T. (2018). Soil resources and element stocks in drylands to face global issues. *Scientific Reports*, *8*(1), 13788. https://doi.org/10.1038/s41598-018-32229-0

Plaza-Bonilla, D., Arrúe, J. L., Cantero-Martínez, C., Fanlo, R., Iglesias, A., & Álvaro-Fuentes, J. (2015). Carbon management in dryland agricultural systems. A review. *Agronomy for Sustainable Development*, *35*(4), 1319–1334. https://doi.org/10.1007/s13593-015-0326-x

Rey, A. (2015). Mind the gap: Non-biological processes contributing to soil CO_2 efflux. *Global Change Biology*, *21*(5), 1752–1761. https://doi.org/10.1111/gcb.12821

Reynolds, J. F., Smith, D. M. S., Lambin, E. F., Turner, B. L., Mortimore, M., Batterbury, S. P. J., Downing, T. E., Dowlatabadi, H., Fernández, R. J., Herrick, J. E., Huber-Sannwald, E., Jiang, H., Leemans, R., Lynam, T., Maestre, F. T., Ayarza, M., & Walker, B. (2007). Global Desertification: Building a Science for Dryland Development. *Science*, *316*(5826), 847–851. https://doi.org/10.1126/science.1131634

Rosenberg, N. J., Blad, B. L., & Verma, S. B. (1983). *Microclimate: The Biological Environment*. John Wiley & Sons.

Serrano-Ortiz, P., Roland, M., Sanchez-Moral, S., Janssens, I. A., Domingo, F., Goddéris, Y., & Kowalski, A. S. (2010). Hidden, abiotic CO2 flows and gaseous reservoirs in the terrestrial carbon cycle: Review and perspectives. *Agricultural and Forest Meteorology*, *150*(3), 321–329. https://doi.org/10.1016/j.agrformet.2010.01.002

Sidari, M., Mallamaci, C., & Muscolo, A. (2008). Drought, salinity and heat differently affect seed germination of *Pinus pinea*. *Journal of Forest Research*, *13*(5), 326–330. https://doi.org/10.1007/s10310-008-0086-4

Topp, G. C., Davis, J. L., & Annan, A. P. (1980). Electromagnetic determination of soil water content: Measurements in coaxial transmission lines. *Water Resources Research*, *16*(3), 574–582. https://doi.org/10.1029/WR016i003p00574

Tu, K., Brooks, P., & Dawson, T. (2001). Using septum-capped vials with continuous-flow isotope ratio mass spectrometric analysis of atmospheric CO2 for Keeling plot applications. *Rapid Communications in Mass Spectrometry*, *15*, 952–956. https://doi.org/10.1002/rcm.320

Wang, X., Wang, J., Xu, M., Zhang, W., Fan, T., & Zhang, J. (2015). Carbon accumulation in arid croplands of northwest China: Pedogenic carbonate exceeding organic carbon. *Scientific Reports*, *5*(1), 11439. https://doi.org/10.1038/srep11439

Zamanian, K., Pustovoytov, K., & Kuzyakov, Y. (2016). Pedogenic carbonates: Forms and formation processes. *Earth-Science Reviews*, *157*, 1–17. https://doi.org/10.1016/j.earscirev.2016.03.003

10. APPENDIX

Appendix Table 1: Exhibits all the irrigations that occurred during the 2021 irrigation season. Dates were often gathered by obvious trends observed from sensors and some were speculated in the field. Bold purple dates are irrigation events that were recorded by sensors, while the blue background cells represent samples that were collected. Measurements include pH, EC, and alkalinity.

#	Source of IRW	IRW Date	Date of collection	pH	EC (µS/cm)	Alk (meq/kg)	$\delta^{18}O$ (‰)
1	IRW-GW1	03/11/2021	-	-	-	-	
2	IRW-GW2	05/02/2021	-	-	-	-	
3	IRW-GW3	05/27/2021	-	-	-	-	
4	IRW-RG1	06/15/2021	6/16/2021	7.75	1093	3.70	-6.68
5	IRW-RG2	07/05/2021	-	-	-	-	
6	IRW-RG3	07/31/2021	7/30/2021	8	1118	3.57	-6.62
7	IRW-RG4	08/29/2021	8/26/2021	8.33	1972	4.72	-6.76
8	IRW-GW4	09/20/2021	9/21/2021	7.42	3880	-	-8.63

Appendix Table 2: Precipitation data from NOAA. A) Is the data from TORNILLO 2 SSE, TX US station, Table B) is the data from JORNADA EXPERIMENTAL RANGE, NM US station.

A. STATION	NAME	DATE	PRCP
USC00419088	TORNILLO 2 SSE, TX US	6/25/2021	0.22
USC00419088	TORNILLO 2 SSE, TX US	6/28/2021	0.78
USC00419088	TORNILLO 2 SSE, TX US	6/29/2021	0.03
USC00419088	TORNILLO 2 SSE, TX US	6/30/2021	0.11
USC00419088	TORNILLO 2 SSE, TX US	7/2/2021	0.03
USC00419088	TORNILLO 2 SSE, TX US	7/3/2021	0.47
USC00419088	TORNILLO 2 SSE, TX US	7/11/2021	0.05
USC00419088	TORNILLO 2 SSE, TX US	7/18/2021	0.07
USC00419088	TORNILLO 2 SSE, TX US	7/23/2021	0.02
USC00419088	TORNILLO 2 SSE, TX US	7/24/2021	0.69
USC00419088	TORNILLO 2 SSE, TX US	7/25/2021	0.11
USC00419088	TORNILLO 2 SSE, TX US	8/1/2021	0.25
USC00419088	TORNILLO 2 SSE, TX US	8/9/2021	0.1
USC00419088	TORNILLO 2 SSE, TX US	8/10/2021	1.55
USC00419088	TORNILLO 2 SSE, TX US	8/12/2021	0.04
USC00419088	TORNILLO 2 SSE, TX US	8/13/2021	0.13
USC00419088	TORNILLO 2 SSE, TX US	8/14/2021	0.1
USC00419088	TORNILLO 2 SSE, TX US	8/15/2021	1.16
USC00419088	TORNILLO 2 SSE, TX US	8/16/2021	0.11
USC00419088	TORNILLO 2 SSE, TX US	8/30/2021	0.65
USC00419088	TORNILLO 2 SSE, TX US	8/31/2021	0.01
USC00419088	TORNILLO 2 SSE, TX US	9/1/2021	0.35
USC00419088	TORNILLO 2 SSE, TX US	9/5/2021	0.02
USC00419088	TORNILLO 2 SSE, TX US	9/24/2021	0.03
USC00419088	TORNILLO 2 SSE, TX US	9/25/2021	0.48
USC00419088	TORNILLO 2 SSE, TX US	9/27/2021	0.2
USC00419088	TORNILLO 2 SSE, TX US	9/30/2021	0.6

B. STATION	NAME	DATE	PRCP
GHCND:USC00294426	JORNADA EXPERIMENTAL RANGE, NM US	8/28/2021	0.03
GHCND:USC00294427	JORNADA EXPERIMENTAL RANGE, NM US	9/1/2021	0.11
GHCND:USC00294428	JORNADA EXPERIMENTAL RANGE, NM US	9/2/2021	0.22
GHCND:USC00294429	JORNADA EXPERIMENTAL RANGE, NM US	9/4/2021	0.13
GHCND:USC00294430	JORNADA EXPERIMENTAL RANGE, NM US	9/16/2021	0.13
GHCND:USC00294431	JORNADA EXPERIMENTAL RANGE, NM US	9/26/2021	0.04
GHCND:USC00294432	JORNADA EXPERIMENTAL RANGE, NM US	9/27/2021	0.27
GHCND:USC00294433	JORNADA EXPERIMENTAL RANGE, NM US	9/29/2021	0.05
GHCND:USC00294434	JORNADA EXPERIMENTAL RANGE, NM US	9/30/2021	0.08
GHCND:USC00294435	JORNADA EXPERIMENTAL RANGE, NM US	10/1/2021	0.08
GHCND:USC00294436	JORNADA EXPERIMENTAL RANGE, NM US	11/25/2021	0.4
GHCND:USC00294437	JORNADA EXPERIMENTAL RANGE, NM US	1/1/2022	0.32
GHCND:USC00294438	JORNADA EXPERIMENTAL RANGE, NM US	1/11/2022	0.07
GHCND:USC00294439	JORNADA EXPERIMENTAL RANGE, NM US	2/3/2022	0.16
GHCND:USC00294440	JORNADA EXPERIMENTAL RANGE, NM US	3/4/2022	0.01
GHCND:USC00294441	JORNADA EXPERIMENTAL RANGE, NM US	3/11/2022	0.07
GHCND:USC00294442	JORNADA EXPERIMENTAL RANGE, NM US	3/22/2022	0.52
GHCND:USC00294443	JORNADA EXPERIMENTAL RANGE, NM US	3/23/2022	0.03
GHCND:USC00294444	JORNADA EXPERIMENTAL RANGE, NM US	3/31/2022	0.01

USDA **Natural Resources Conservation Service**

Web Soil Survey
National Cooperative Soil Survey

4/29/2023
Page 1 of 3

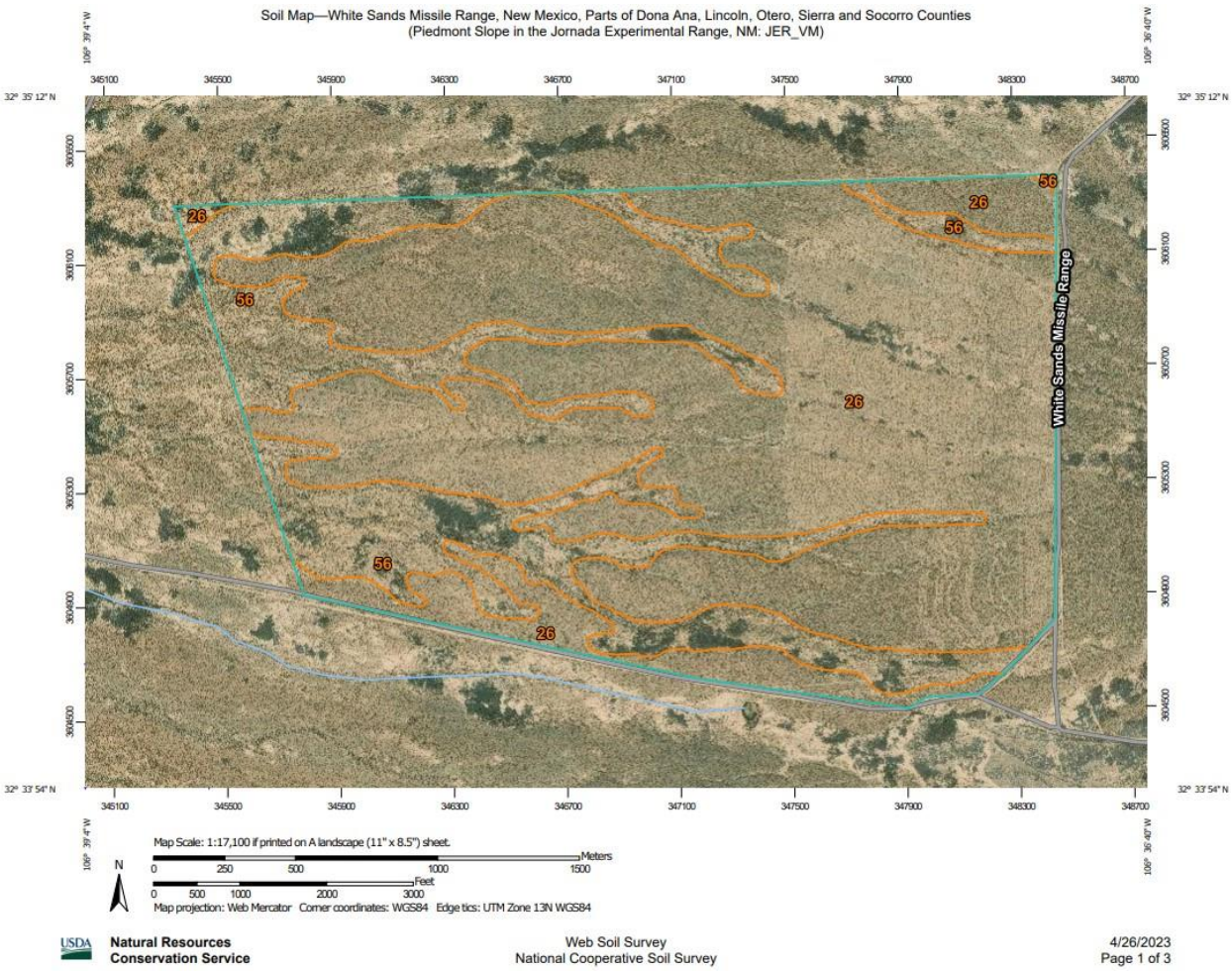

Appendix Figure 1: Soil maps of the study areas displaying contrasting soil variability: A) The Pecan Orchard site displays more variability with six different soil units, including the dominant Saneli silty clay loam (Sa) covering 52% of the area, followed by Tigua silty clay (Tg) at 25.5% and Harkey silty clay loam (Hk) at 15%. Our Pecan_Coarse site is within the Glendale silty clay loam (Ge) unit, while Pecan_Fine is within the Tigua silty clay (Tg) unit. B) The Jornada Experimental Range piedmont slope is composed of only two units, with the Doña Ana-Chutum complex covering 74% of the study area, where our sensors and gas samplers are located, and the Mimbres-Chutum-Ybar complex, covering 26% of the area, with 0 to 5% slopes.

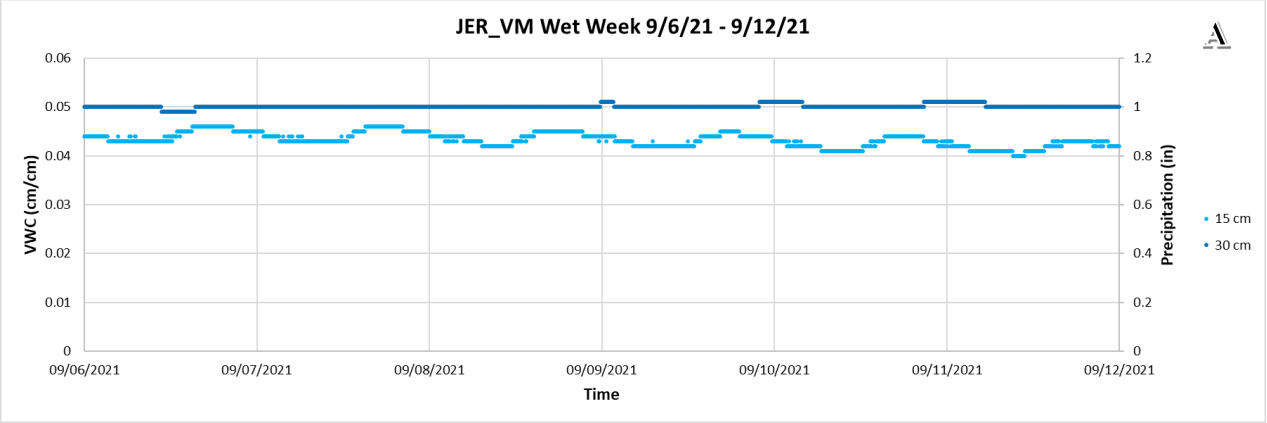
JER_VM Wet Week 9/6/21 - 9/12/21
A
VWC (cm/cm)
Precipitation (in)
0.06
0.05
0.04
0.03
0.02
0.01
0
1.2
1
0.8
0.6
0.4
0.2
0
09/06/2021
09/07/2021
09/08/2021
09/09/2021
09/10/2021
09/11/2021
09/12/2021
Time
15 cm
30 cm

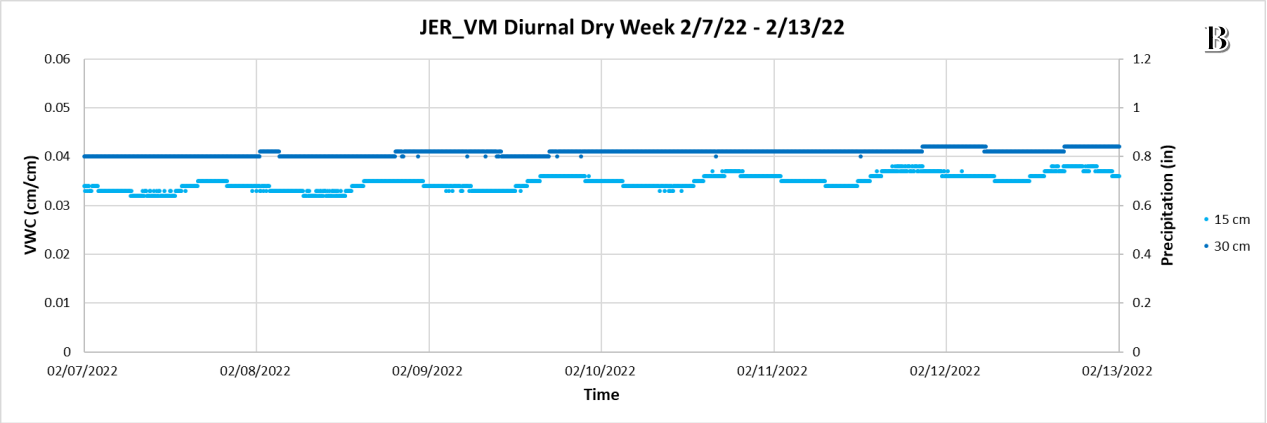
JER_VM Diurnal Dry Week 2/7/22 - 2/13/22
B
VWC (cm/cm)
Precipitation (in)
0.06
0.05
0.04
0.03
0.02
0.01
0
1.2
1
0.8
0.6
0.4
0.2
0
02/07/2022
02/08/2022
02/09/2022
02/10/2022
02/11/2022
02/12/2022
02/13/2022
Time
15 cm
30 cm

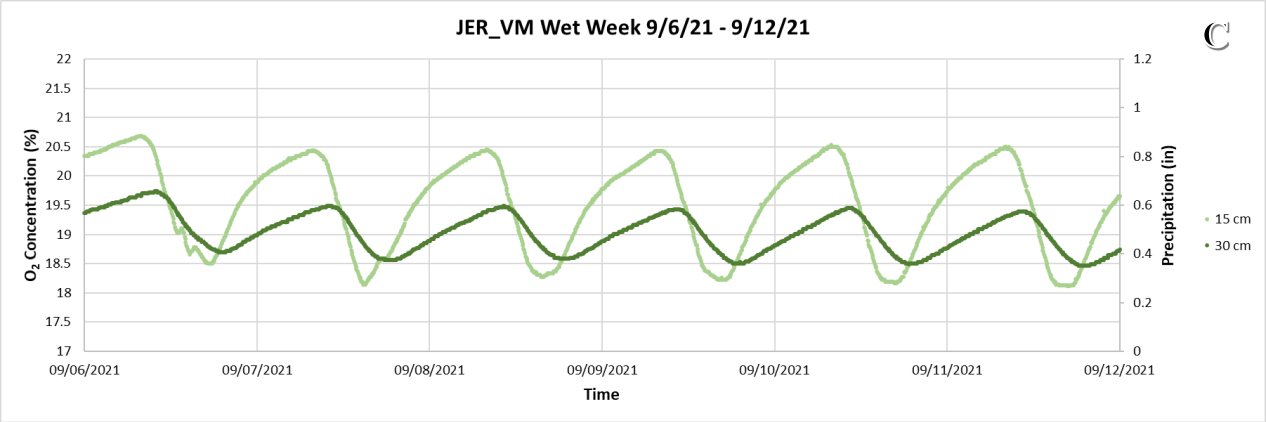
JER_VM Wet Week 9/6/21 - 9/12/21
C
O2 Concentration (%)
Precipitation (in)
22
21.5
21
20.5
20
19.5
19
18.5
18
17.5
17
1.2
1
0.8
0.6
0.4
0.2
0
09/06/2021
09/07/2021
09/08/2021
09/09/2021
09/10/2021
09/11/2021
09/12/2021
Time
15 cm
30 cm

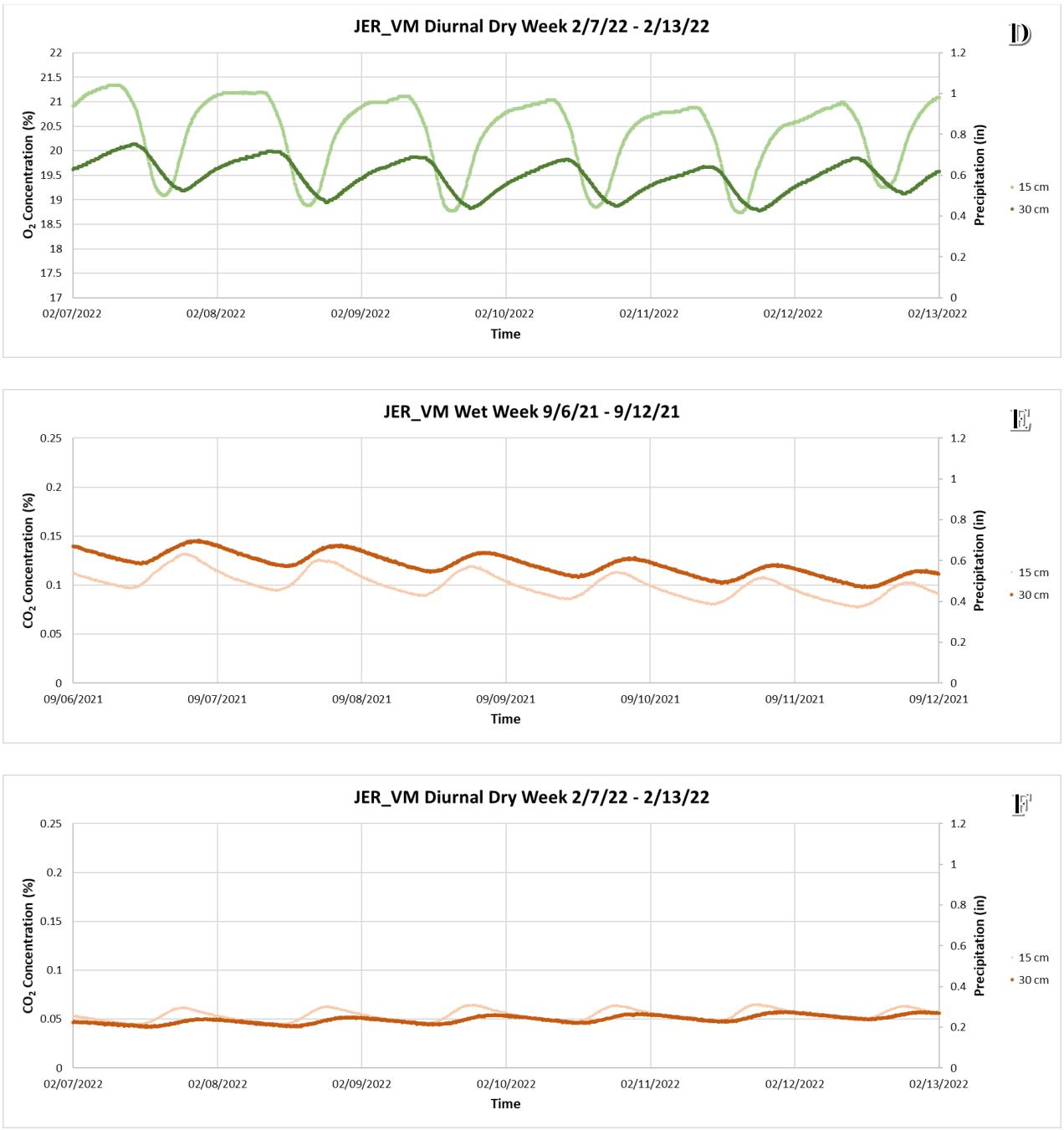

Appendix Figure 2: We observed diurnal variations at the JER_VM site. The wet week was from 9/6/21 to 9/12/21, while our dry week was from 2/7/22 to 2/13/22. The time Increments display dates all at 12:00 AM MST. Panel A) and B) in blues display soil moisture. Panel C) and D) in greens display O_2, and finally E) and F) in orange and beige display CO_2.

11. VITA

Valeria Isabel Molina was born in El Paso, Texas to Mayela Carrillo and Hector Molina. Her parents were born in Chihuahua, Mexico. She attended an international elementary and middle school where she learned three languages: Spanish, English, and German. In 6th grade, she was an exchange student, who stayed with a foster family in Reinheim, Germany. Valeria attended Del Valle high school initially pursuing the Multinational Business Academy (MBA) and received dual credit. She attained her associate's degree from the El Paso Community College in General Sciences. In 2018, Valeria was accepted to the Geological Sciences program at The University of El Paso Texas. Valeria conducted research as an undergraduate student under the mentoring of Dr. Brunner. Her research included the extraction of accessory minerals from rocks adjacent to salt domes in Gypsum Valley, Colorado, for which she utilized petrographic microscopy. In 2021, she received her Bachelor's in Geological Sciences with Magna Cum Laude honors and Fast-Track Dual Credit (BS/MS); she soon began as a Research Assistant during the summer, collecting field data for the Dryland Critical Zone project. The data collection build into her Master's Thesis project. She was a Reaserseach Assitant until her last semester at UTEP, Valeria was a Teaching Assistant that led laboratory assignments in a laboratory and field setting within the Department of Earth, Environmental, and Resource Sciences (DEERS). Throughout her time as a UTEP student, she was part of multiple student organizations; she often volunteered and helped organize events for her department.

Contact Information: vimolina2@miners.utep.edu